Cancer Cell

Report

Mutant IDH inhibitors induce lineage differentiation in IDH-mutant oligodendroglioma

Graphical abstract

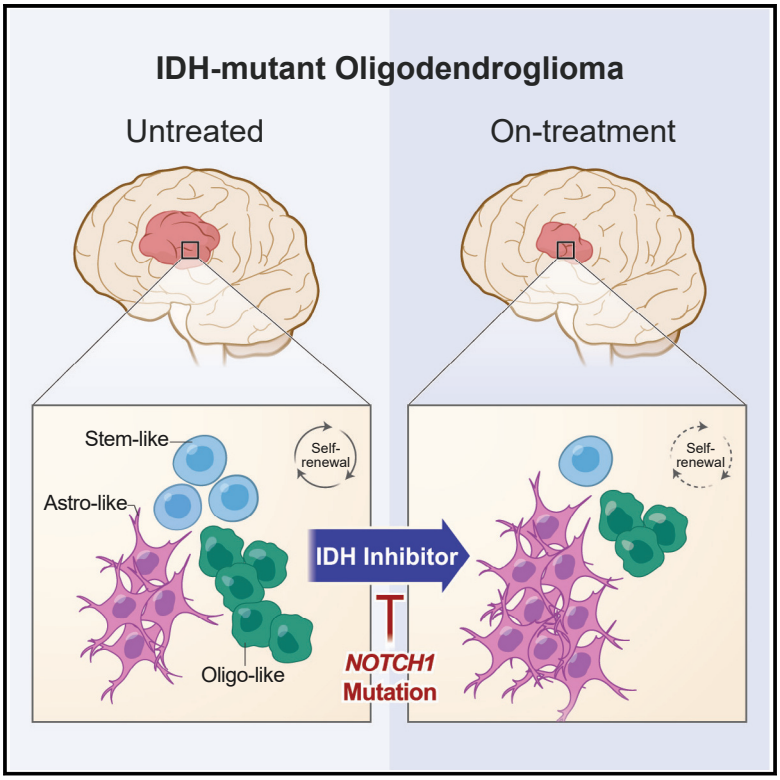

Highlights

- Single-cell analysis of on-treatment gliomas reveals cellular basis of drug responses
- In responders, mutant IDH inhibitors induce lineage differentiation
- The differentiation favors astrocytic-like over stem/progenitor-like states
- NOTCH1 mutations modify the response and may serve to stratify patients

Authors

Avishay Spitzer, Simon Gritsch, Masashi Nomura, ..., Daniel P. Cahill, Mario L. Suvà, Itay Tirosh

Correspondence

keith_ligon@dfci.harvard.edu (K.L.L.), cahill@mgh.harvard.edu (D.P.C.), suva.mario@mgh.harvard.edu (M.L.S.), itay.tirosh@weizmann.ac.il (I.T.)

In brief

The molecular response of IDH-mutant glioma to mutant IDH inhibitors is poorly understood. Spitzer et al. show that, in patients with clinical response, mutant IDH inhibitors induce lineage differentiation of cancer cells and deplete cells in a stem/progenitor-like state. They further highlight potential modifiers of such differentiation response in glioma.

Spitzer et al., 2024, Cancer Cell *42*, 1–11
May 13, 2024
https://doi.org/10.1016/j.ccell.2024.03.008

CellPress

Please cite this article in press as: Spitzer et al., Mutant IDH inhibitors induce lineage differentiation in IDH-mutant oligodendroglioma, Cancer Cell (2024), https://doi.org/10.1016/j.ccell.2024.03.008

Cancer Cell

CellPress

Report

Mutant IDH inhibitors induce lineage differentiation in IDH-mutant oligodendroglioma

Avishay Spitzer,[1,2,3,20] Simon Gritsch,[4,5,18,20] Masashi Nomura,[4,5,20] Alexander Jucht,[4,5] Jerome Fortin,[6,7] Ramya Raviram,[8,9] Hannah R. Weisman,[4,5] L. Nicolas Gonzalez Castro,[4,5,14,18] Nicholas Druck,[4,5] Rony Chanoch-Myers,[1] John J.Y. Lee,[4,5] Ravindra Mylvaganam,[4] Rachel Lee Servis,[4] Jeremy Man Fung,[4] Christine K. Lee,[11] Hiroaki Nagashima,[11] Julie J. Miller,[12] Isabel Arrillaga-Romany,[10] David N. Louis,[4] Hiroaki Wakimoto,[11] Will Pisano,[13] Patrick Y. Wen,[14] Tak W. Mak,[6,15,16] Marc Sanson,[17] Mehdi Touat,[17,18] Dan A. Landau,[8,9] Keith L. Ligon,[5,13,19,21,*] Daniel P. Cahill,[11,21,*] Mario L. Suvà,[4,5,21,*] and Itay Tirosh[1,21,22,*]

[1]Department of Molecular Cell Biology, Weizmann Institute of Science, Rehovot 761001, Israel
[2]Department of Oncology, Tel Aviv Sourasky Medical Center, Tel Aviv, Israel
[3]Faculty of Medicine, Tel Aviv University, Tel Aviv, Israel
[4]Department of Pathology and Center for Cancer Research, Massachusetts General Hospital and Harvard Medical School, Boston, MA 02114, USA
[5]Broad Institute of Harvard and MIT, Cambridge, MA 02142, USA
[6]Princess Margaret Cancer Centre, University Health Network, Toronto, ON M5G 2C1, Canada
[7]Department of Neurology and Neurosurgery, Montreal Neurological Institute-Hospital, McGill University, Montreal, Canada
[8]New York Genome Center, New York, NY, USA
[9]Weill Cornell Medicine, New York, NY, USA
[10]Departments of Neurology and Radiation Oncology, Division of Hematology/Oncology, Massachusetts General Hospital Cancer Center, Harvard Medical School, Boston, MA 02114, USA
[11]Department of Neurosurgery, Massachusetts General Hospital and Harvard Medical School, Boston, MA 02114, USA
[12]Pappas Center for Neuro-Oncology, Department of Neurology, Massachusetts General Hospital, Harvard Medical School, Boston, MA 02114, USA
[13]Department of Pathology, Brigham and Women's Hospital, Boston, MA, USA
[14]Center for Neuro-Oncology, Dana-Farber Cancer Institute, Harvard Medical School, Boston, MA 02215, USA
[15]Centre for Oncology and Immunology, Hong Kong Science Park, Hong Kong SAR, China
[16]Department of Pathology, School of Clinical Medicine, Li Ka Shing Faculty of Medicine, The University of Hong Kong, Hong Kong SAR, China
[17]Sorbonne Université, Inserm, CNRS, UMR S 1127, Institut du Cerveau, ICM, AP-HP, Hôpitaux Universitaires La Pitié Salpêtrière - Charles Foix, Service de Neurologie 2-Mazarin, Paris, France
[18]Department of Neurology, Brigham and Women's Hospital, Boston, MA, USA
[19]Department of Pathology, Dana-Farber Cancer Institute, Boston, MA, USA
[20]These authors contributed equally
[21]These authors contributed equally
[22]Lead contact
*Correspondence: keith_ligon@dfci.harvard.edu (K.L.L.), cahill@mgh.harvard.edu (D.P.C.), suva.mario@mgh.harvard.edu (M.L.S.), itay.tirosh@weizmann.ac.il (I.T.)
https://doi.org/10.1016/j.ccell.2024.03.008

SUMMARY

A subset of patients with IDH-mutant glioma respond to inhibitors of mutant IDH (IDHi), yet the molecular underpinnings of such responses are not understood. Here, we profiled by single-cell or single-nucleus RNA-sequencing three IDH-mutant oligodendrogliomas from patients who derived clinical benefit from IDHi. Importantly, the tissues were sampled on-drug, four weeks from treatment initiation. We further integrate our findings with analysis of single-cell and bulk transcriptomes from independent cohorts and experimental models. We find that IDHi treatment induces a robust differentiation toward the astrocytic lineage, accompanied by a depletion of stem-like cells and a reduction of cell proliferation. Furthermore, mutations in *NOTCH1* are associated with decreased astrocytic differentiation and may limit the response to IDHi. Our study highlights the differentiating potential of IDHi on the cellular hierarchies that drive oligodendrogliomas and suggests a genetic modifier that may improve patient stratification.

Please cite this article in press as: Spitzer et al., Mutant IDH inhibitors induce lineage differentiation in IDH-mutant oligodendroglioma, Cancer Cell (2024), https://doi.org/10.1016/j.ccell.2024.03.008

INTRODUCTION

Hotspot mutations at isocitrate dehydrogenase (IDH) genes, $IDH1^{R132}$ and $IDH2^{R172}$, have been identified in a diverse spectrum of human malignancies, including diffuse gliomas.[1–5] These mutations lead to over-accumulation of the oncometabolite R-2-hydroxyglutarate (2HG),[6] which promotes tumorigenesis by inhibiting α-ketoglutarate-dependent dioxygenases, such as histone and DNA demethylases,[7,8] thereby altering the cellular epigenetic states.[9–12]

Several small-molecule inhibitors of mutant IDH (IDHi) are currently in clinical assessment. In glioma, limited activity was observed in patients with high-grade disease and in *in vitro* cell culture models.[13–16] However, a phase 3 clinical trial[17] (INDIGO trial, NCT04164901) recently demonstrated that treatment with the IDHi vorasidenib induces objective radiographic response in 10.7% of patients, and significantly improves progression-free survival in patients with residual or recurrent IDH mutant grade 2 gliomas. The molecular bases of these responses remain uncharacterized and would need to be elucidated in order to (1) identify the molecular modifiers of such responses; (2) better select the patients most likely to benefit; and (3) identify potential synergies.

RESULTS

To examine the molecular underpinnings of responses to IDHi, we analyzed four oligodendroglioma samples isolated from three patients as part of the NCT03343197 phase 1 trial that had evidence of clinical benefit (see Table S1 for clinical information, Figures 1A and 1B for study overview and timelines).[18] Patient MGH170 showed partial response by Response Assessment in Neuro-Oncology (RANO) criteria after 10 months of treatment with vorasidenib and remained clinically and radiographically stable after 60 months from treatment initiation. Patient MGH229 showed stable disease without progression on imaging after 55 months of ivosidenib treatment. According to the trial protocol, tumor tissue was obtained from MGH170 and MGH229 on-treatment 4 weeks after initiation of IDHi. These samples were profiled by single-cell RNA-sequencing (scRNA-seq) using the SMART-Seq2 protocol.[19] Overall, 1,153 cells passed our stringent quality controls, with 4,333 genes detected per cell on average.

We further profiled a matched pair of frozen samples (pre- and on-treatment, 4 weeks after treatment initiation) from a third oligodendroglioma patient (BWH445) who gained clinical benefit from IDHi treatment by single-nucleus RNA-sequencing (snRNA-seq, 10x genomics). Patient BWH445 showed stable disease without evidence of progression on imaging 66 months from initiation of ivosidenib treatment (Figure 1B; Table S1). Overall, 8,793 nuclei passed quality control with 2,816 genes detected on average.

The two IDHi-treated samples profiled using scRNA-seq were combined with scRNA-seq from six treatment-naive grade 2 oligodendrogliomas,[20,21] whereas the matched pair was analyzed separately from this cohort by comparing the two time points (Figure 1C). Malignant oligodendroglioma cells were clearly distinguishable from the immune and glial cells by inferred copy number aberrations (CNA), including the co-deletion of chromosome arms 1p/19q, and by expression of marker genes (Figures S1A–S1C; Table S2).[20]

IDHi treatment affects lineage-defining gene sets

Comparison between IDHi-treated and untreated samples (non-paired samples) using gene set enrichment analysis (GSEA) identified 230 significantly enriched gene-sets (Figure 2A; Table S3). These included gene-sets defining the three components of the cellular hierarchy that we previously proposed for oligodendroglioma: proliferating cells resembling neural progenitor cells (NPC-like) and cells differentiated toward the astrocytic (AC-like) and oligodendrocytic (OC-like) lineages.[20] The most highly enriched gene-sets in IDHi-treated samples were those of the AC-like states defined previously in glioma and gene-sets of normal astrocytes.[20–28] Conversely, the most highly enriched gene-sets in the untreated samples were of the OC-like state in glioma.

Of the genes with highest fold changes, AC-like genes accounted for a large fraction of the upregulated genes, while OC-like and NPC-like genes accounted for a large fraction of the downregulated genes (Figure 2B). Specifically, 457 genes defining the AC-like, OC-like, and NPC-like states together accounted for 53% of the 102 most differentially expressed genes (DEGs), with an average of 4-fold expression difference, compared with only 4.7% expected by chance ($p = 4.92^{-15}$, hypergeometric test). Comparison between the pre- and on-treatment samples of BWH445 revealed a similar enrichment of astrocytic gene-sets upon IDH inhibition (Figure 2C). Moreover, when intersecting the DEG lists of the unmatched and matched cohorts we found that shared genes were enriched with upregulated AC-like genes (e.g., *AQP4*, *CST3*; observed 41/81 vs. expected 1/81, $p = 1.33^{-14}$, one-sided hypergeometric test) and with downregulated OC-like (e.g., *SOX8*; 18/71 vs. 1/71, $p = 1.26^{-5}$) and NPC-like (e.g., *DCX*, *ASCL1*; 9/71 vs.1/71, $p = 0.009$) genes (Figure 2D). Thus, *in vivo* IDH inhibition primarily impacts these neurodevelopmental programs.

IDHi-treated samples are enriched with AC-like cells

Importantly, these DEGs were highly expressed only in specific subsets of cells that were all found in both conditions (Figures 3A and 3B). Thus, IDHi treatment results in changes in the proportions of pre-existing cellular states (AC-like, OC-like, and NPC-like), as well as of an intermediate "undifferentiated" state and of cycling cells (Figures S1D and S1E). IDHi-treated samples had the largest proportion of AC-like cells ($p = 0.02$, one-sided t test), the smallest proportion of cells classified as either undifferentiated or NPC-like ($p = 0.002$) and the smallest proportion of cycling cells ($p = 0.01$). This pattern was largely evident in any pairwise comparison between an IDHi-treated and untreated samples (Figure S2A). Comparison of the matched pre- and on-treatment BWH445 samples revealed a 2-fold increase in the proportions of both AC-like and OC-like cells and a 4-fold decrease in the proportion of cycling cells (Figures 3C, 3D, and S2B–S2D).

We also profiled by sc/snRNA-seq six samples from four IDH-mutant astrocytoma patients that were treated with IDHi and progressed while on treatment (Table S1), including two matched pairs. These samples did not show an increase in lineage differentiation as observed in the oligodendroglioma cohort (Figures S3A–S3H). However, since those four patients all had astrocytoma, it is difficult to interpret their differences from our cohort of responders given these biologically distinct diseases.

We confirmed our observations by RNA *in situ* hybridization with markers of AC-like cells (*GFAP* and *ALDOC*), NPC-like cells

Please cite this article in press as: Spitzer et al., Mutant IDH inhibitors induce lineage differentiation in IDH-mutant oligodendroglioma, Cancer Cell (2024), https://doi.org/10.1016/j.ccell.2024.03.008

CellPress

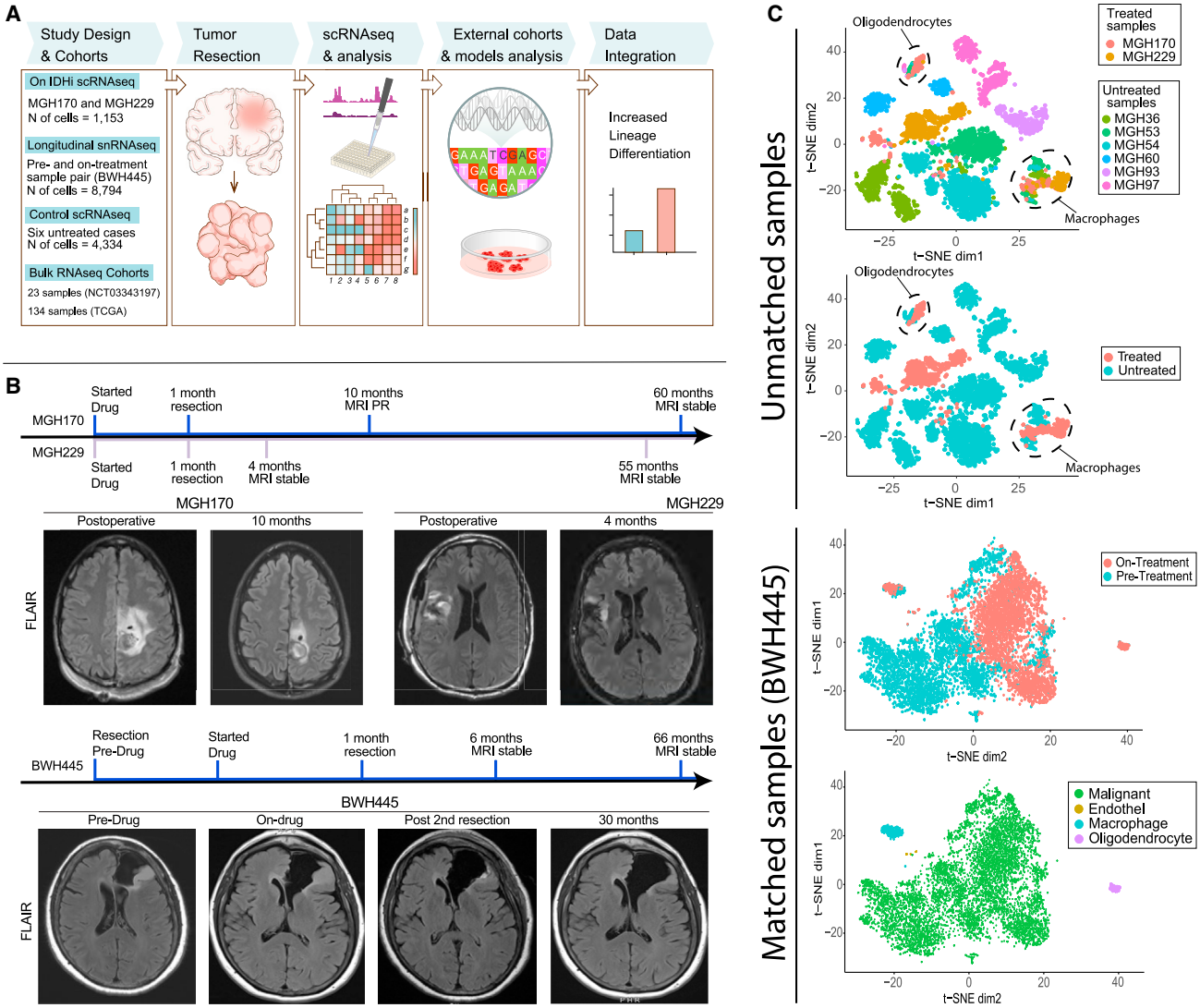

Figure 1. Study workflow, clinical timeline, and dataset overview

(A) Scheme describing the study workflow.

(B) Top panel shows an overview of the clinical history of MGH170 and MGH229 after initiation of IDHi treatment as well as representative brain MRIs of the two patients treated with IDHi. Bottom panel shows the clinical history of BWH445 before and after initiation of IDHi therapy as well as representative brain MRIs of this patient.

(C) t-distributed stochastic neighbor embedding (t-SNE) plots of the unmatched samples showing 5,487 single cell expression profiles and of the matched on- and pre-treatment samples showing 8,219 single nucleus expression profiles.

See also Figure S1 and Tables S1 and S2.

(*SOX4*), and cell proliferation (Ki-67) (Figures 3E, 3F, and S4A) in the pre- and on-treatment matched samples, in two IDHi-treated unmatched samples, in a sample of MGH229 long before IDHi treatment (MGH229pre), and in seven untreated oligodendroglioma samples. Moreover, when comparing cells classified into the same state, we noticed differences between IDHi-treated and untreated cells that supported an induction of differentiation by IDHi. Cells classified as AC-like in IDHi-treated samples (MGH170 and MGH229) were enriched with gene-sets reflecting normal astrocytic development, compared to AC-like cells in the untreated samples (Figure S4B). Thus, IDHi may promote both an increased *proportion* of AC-like cells and an increased *degree* of differentiation, such that AC-like differentiation in IDHi-treated samples better recapitulates the normal astrocytic state. A similar pattern was observed for OC-like cells, which displayed enrichment of normal oligodendrocytic gene-sets[22–27] in IDHi-treated vs. untreated samples (Figures S4C and S4D). However, unlike the consistent increase in AC-like differentiation across IDHi-treated samples, the effect on OC-like differentiation appears to be variable (Figure S4).

Taken together, these results suggest that clinical benefit from IDHi treatment is associated with cellular differentiation, and more specifically with an increase in the fraction and degree of

Please cite this article in press as: Spitzer et al., Mutant IDH inhibitors induce lineage differentiation in IDH-mutant oligodendroglioma, Cancer Cell (2024), https://doi.org/10.1016/j.ccell.2024.03.008

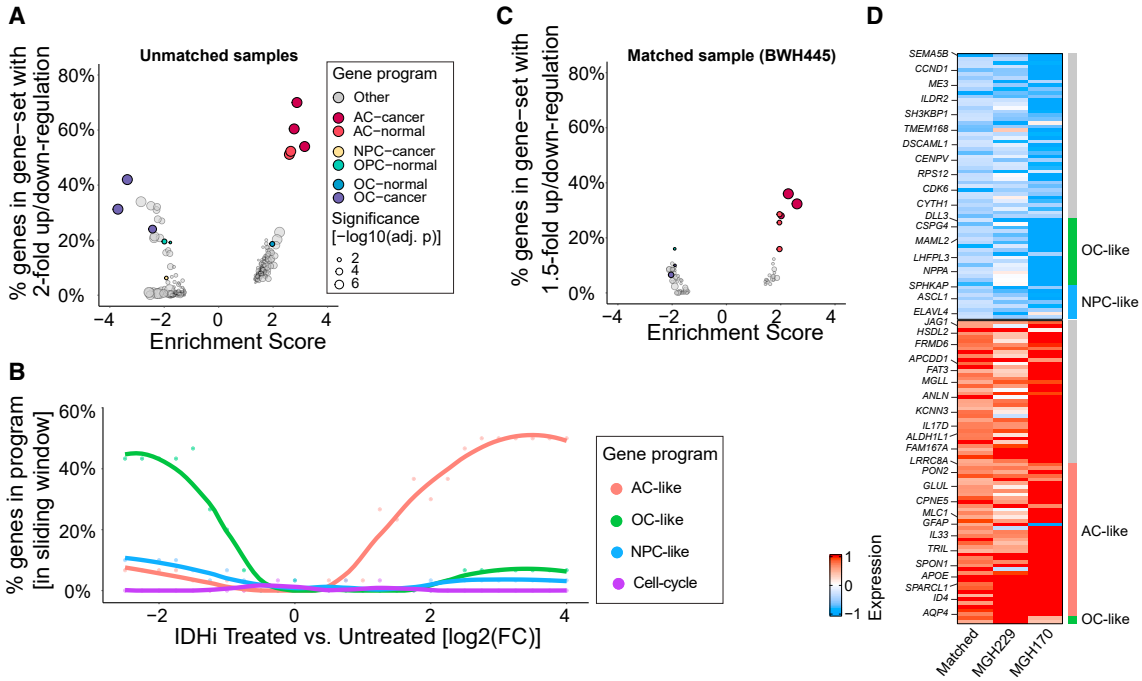

Figure 2. Gene set enrichment analysis

(A) Comparison of IDHi-treated and untreated (unmatched) samples using GSEA. Each dot represents a gene-set that passed the statistical significance threshold (adjusted p value < 0.05, permutation test), dot size represents the extent of significance and color indicates whether the gene-set belongs to a glioma hierarchy/neural development gene-set. X axis shows the GSEA normalized enrichment score (NES), Y axis shows the fraction of genes in each gene-set with an absolute $\log_2$-ratio>1 (e.g., genes at the extreme ends of the ranked list used for GSEA computation with more than a 2-fold change).

(B) Enrichment of the ranked list used for GSEA (unmatched samples). Dots represent the percentage of genes, in a sliding window of 30 genes (by $\log_2$-ratio values), that overlap each of the three expression programs and the cell cycle. Trend line was computed using LOESS regression.

(C) Comparison of matched on- and pre-treatment samples using GSEA (same as panel A). Y axis shows the fraction of genes in each gene-set with an absolute $\log_2$-ratio>$\log_2$(1.5).

(D) Common genes of the most highly DEGs (computed separately for the unmatched and matched cohorts). Columns represent samples, rows represent DEGs, which are annotated by the associated expression programs. The expression values of the unmatched samples are shown relative to the average bulk expression profile of the untreated samples and those of the matched on-treatment sample are shown relative to the expression profile of its pre-treatment counterpart. See also Figure S2 and Table S3.

differentiation of AC-like cells, and a decrease in the proportion of undifferentiated and proliferating cells.

Validations in independent cohorts

The small size of our cohort and the unique clinical course of each patient (Table S1) are inherent limitations of our study. The capacity to profile human glioma tissue on-treatment has been a major long-term constraint in clinical trials due to limited indication for such on-drug sampling.[29] Additionally, only a small subset of patients showed signs of radiographic responses, making acquisition of those specific on-treatment samples even more challenging. To partially overcome these limitations, we next extended our analysis to relevant external datasets.

First, we examined 23 oligodendroglioma bulk RNA-seq profiles from a perioperative phase 1 trial[30] of ivosidenib and vorasidenib. Consistent with our previous observations, we found significantly higher AC-like differentiation and lower cell cycle activity in IDHi-treated compared to untreated samples (Figure 4A). Moreover, we observed a significant negative association between AC-like differentiation and cell cycle activity (Pearson's r = −0.58, p = 0.004, t test, Figure 4B). This dataset is mainly limited by the number of untreated samples (two). Therefore, to more comprehensively examine untreated oligodendrogliomas, we next leveraged the The Cancer Genome Atlas (TCGA) low-grade glioma cohort that includes 134 oligodendroglioma bulk RNA-seq profiles. We observed in this dataset as well a significant negative association between AC-like differentiation and cell cycle activity (Pearson's r = −0.35, p = 4.15^{-5}, t test); however, this association was significantly weaker in untreated relative to treated samples (Figure S5A), suggesting that IDHi treatment promotes AC-like differentiation while inhibiting cell cycle, thereby strengthening their negative association.

We compared the AC-like differentiation scores of the TCGA cohort to those of our scRNA-seq cohort, when averaging across the cells in each tumor (Figure S5B). As expected, the IDHi-treated samples were highly AC-like differentiated even when compared to 134 untreated TCGA samples (Figure S5C). Specifically, MGH170 (partial clinical response) was the most AC-differentiated among all samples, whereas MGH229 (stable disease) was within the top 3% of AC-differentiated samples (4 out of 134). By comparison, our untreated samples analyzed by scRNA-seq spanned the expected spectrum of AC-like differentiation within the TCGA cohort. Taken together, these results support the hypothesis that treatment of oligodendroglioma

Please cite this article in press as: Spitzer et al., Mutant IDH inhibitors induce lineage differentiation in IDH-mutant oligodendroglioma, Cancer Cell (2024), https://doi.org/10.1016/j.ccell.2024.03.008

CellPress

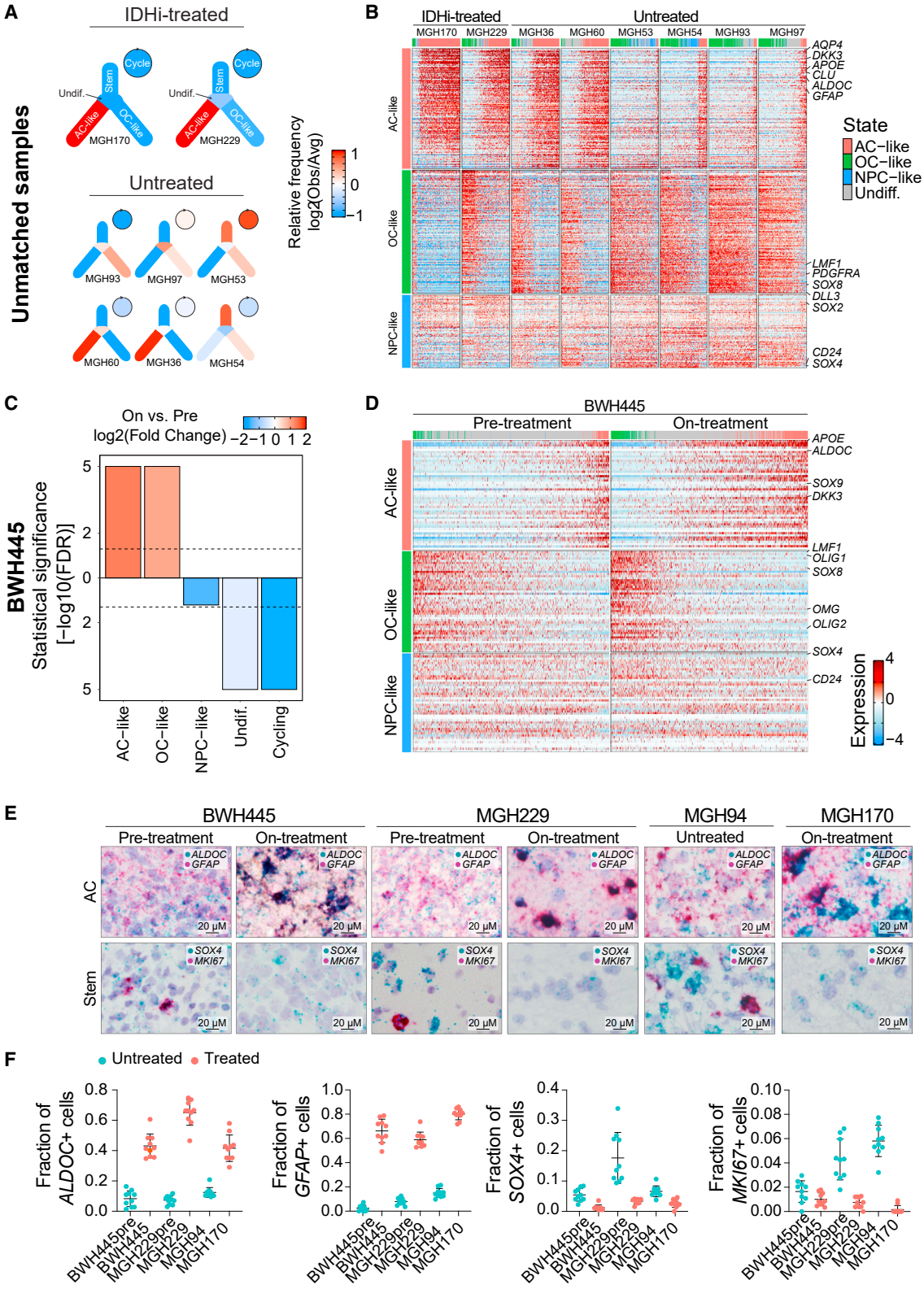

Figure 3. IDHi treatment is associated with AC differentiation

(A) Scheme depicting a model of cellular hierarchy in which colors represents the relative frequency of each cellular state in each tumor sample of the unmatched cohort.

(legend continued on next page)

Please cite this article in press as: Spitzer et al., Mutant IDH inhibitors induce lineage differentiation in IDH-mutant oligodendroglioma, Cancer Cell (2024), https://doi.org/10.1016/j.ccell.2024.03.008

with IDHi induces lineage differentiation toward the AC-like phenotype and decreases the proliferative capacity of the malignant cells.

In-vitro model supports IDHi-induced astrocytic differentiation

We sought to validate our findings *in vitro* and to further investigate the mechanisms of response to IDHi. As cell lines are notoriously difficult to derive from IDH-mutant glioma, we utilized glioma cells derived from an engineered *Idh1*$^{LSL\text{-}R132H}$;*Trp53*$^{flox/flox}$;*Olig2*^{Cre} mouse[31] (STAR Methods). This model was profiled using scRNA-seq (10x Genomics) when cultured with or without the IDHi AG-881 (vorasidenib). As in patient samples, IDHi-treatment led to enrichment of astrocytic gene-sets and depletion of cell cycle gene-sets (Figure 4C). Accordingly, IDHi-treated cells had a significant increase in the proportion of AC-like cells (12.8% vs. 7.5%, p = 0.0001, hypergeometric test) and a significant decrease in the proportions of NPC-like and cycling cells (3.7% vs. 7% and 31.3% vs. 39.7%, respectively, p < 0.001, hypergeometric test) (Figure 4D).

Consistent changes in methylation and gene expression

Next, we wondered if IDHi treatment was associated with a reversal of the global DNA hypermethylation that occurs in IDH-mutant glioma and that may play a role in tumorigenesis.[9–12] To elucidate this, we concurrently profiled from the same single cells (multi-omics) the DNA methylome and the transcriptome of IDHi treated and untreated mouse *Idh1*$^{LSL\text{-}R132H}$;*Trp53*$^{flox/flox}$;*Olig2*^{Cre} glioma cells.[32,33] As expected, we found a significant global decrease of DNA methylation in the IDHi treated cells, compared to the matched untreated cells (Figure 4E, p = 0.004, one-sided Kolmogorov-Smirnov test), albeit of modest fold-change.

We next focused on changes in promoter methylation, as these may be linked to gene regulation. Overall, changes in promoter DNA methylation did not correlate significantly with changes in gene expression of the respective genes (Pearson's r = −0.005, p = 0.7, t test), highlighting the difficulty in pinpointing the causes of expression changes directly from analysis of DNA methylation. Nevertheless, the enrichment of functional gene-sets with demethylated genes, in treated vs. untreated cells, was significantly correlated with their enrichment with upregulated genes (Pearson's r = 0.58, p < 2.2^{-16}, t test, Figure 4F; Table S4). In particular, 10 gene-sets were significantly enriched (p < 0.05) both with demethylated genes and with upregulated genes. Strikingly, four out of the ten gene-sets reflect astrocytic differentiation (p < 10^{-6}, bootstrapping). Thus, despite weak association between changes in methylation and in expression at the level of individual genes, we find a consistent functional effect, with convergence to AC-related gene-sets.

Putative modifiers of AC-like differentiation

Our observation that inhibiting the activity of a driver mutation induces differentiation is consistent with a model of gliomagenesis through a block of differentiation.[10,34] Notably, induction of differentiation could provide clinical benefits that may not be adequately assessed by radiographic measures of response that have been designed for cytotoxic drugs, which could potentially explain some of the controversy around the efficacy of IDHi.[13–16,35] Indeed, radiographic response to IDHi has thus far been observed in a minor subset of IDH-mutant glioma, highlighting the need of predicting which patients will derive clinical benefit.

Since optimal response to IDHi may require plasticity along AC-like differentiation states, pre-existing diversity of such states in untreated samples may predict the capacity for further differentiation and hence the response to IDHi. AC differentiation is decreased in gliomas with increased grade[21] (Figure S5B), consistent with the increased response rate observed in non-enhancing compared to enhancing IDH-mutant glioma,[18] as well as with the stronger effect that we observed in MGH170 (grade 2) compared with MGH229 (grade 3). Given this potential significance of AC differentiation, we examined if particular mutations correlate with AC differentiation in TCGA. We found that *NOTCH1* mutations are associated with a low degree of AC-like differentiation in grade 2 oligodendroglioma (Figures 4G, 4H, S5D, and S5E; Table S5), suggesting that *NOTCH1* mutations may serve as a biomarker for IDHi response. Notably, neither AC-like differentiation nor *NOTCH1* mutation status are associated with a more indolent disease course (Figure S5F), suggesting a potentially specific link to IDHi response.

To examine the effect of *NOTCH1* on IDHi response, we knocked-out (KO) *Notch1* in the *in vitro* mouse model described previously. Cells were transduced with a mix of two *Notch1*-targeting sgRNAs or *ROSA26* sgRNA (control), collected 4 days post-transduction and profiled using scRNA-seq, with or without IDHi treatment (by AG-881). While IDHi robustly induced AC-like differentiation in patient samples and in *Notch1*-WT mouse cells, this was not observed in *Notch1*-KO cells. Specifically, we did not detect a significant enrichment of astrocytic gene-sets or an increase in the proportion of AC-like cells in IDHi-treated vs. untreated samples (Figures 4I and 4J). We did detect, however, a significant decrease in the proportion of NPC-like or cycling cells, suggesting a partial response to treatment. Interestingly, the negative effect of *Notch1*-KO on expression of AC lineage markers was

(B) Relative expression of genes associated with the AC-like, OC-like, and NPC-like programs across the unmatched samples. Cells are ordered by AC-like score minus OC-like score; genes are ordered by expression log2-ratio. For visualization, each tumor was randomly down-sampled to 130 cells.
(C) Comparison of the fraction of cells assigned to each state between the on- and pre-treatment matched samples. Bar values represent the statistical significance of each pairwise comparison, defined as -log10 of a p value calculated by hypergeometric test and corrected for multiple testing using the Benjamini-Hochberg method; bar direction (up or down) is defined by an increase or decrease, respectively, of the relevant state fraction in the on-treatment sample. Bar colors represent the relative change in state fractions.
(D) Same as (B) for the matched pair (no down-sampling in this case).
(E) *In situ* RNA hybridization of tumors BWH445 (pre-treatment and on-treatment), MGH229 (pre-treatment and on-treatment), MGH94 (untreated), and MGH170 (on-treatment) for AC-like (*GFAP*, *ALDOC*), Stem-like (*SOX4*), and proliferation (Ki67) markers.
(F) The fraction of cells staining positive for *GFAP*, *ALDOC*, *SOX4*, and Ki67 based on RNA *in situ* hybridization of tumors BWH445, MGH229, MGH94, and MGH170. Each dot corresponds to one field of view. Horizontal line represents the mean, error bar ± 1SD.
See also Figures S1–S4, Table S1.

Please cite this article in press as: Spitzer et al., Mutant IDH inhibitors induce lineage differentiation in IDH-mutant oligodendroglioma, Cancer Cell (2024), https://doi.org/10.1016/j.ccell.2024.03.008

CellPress

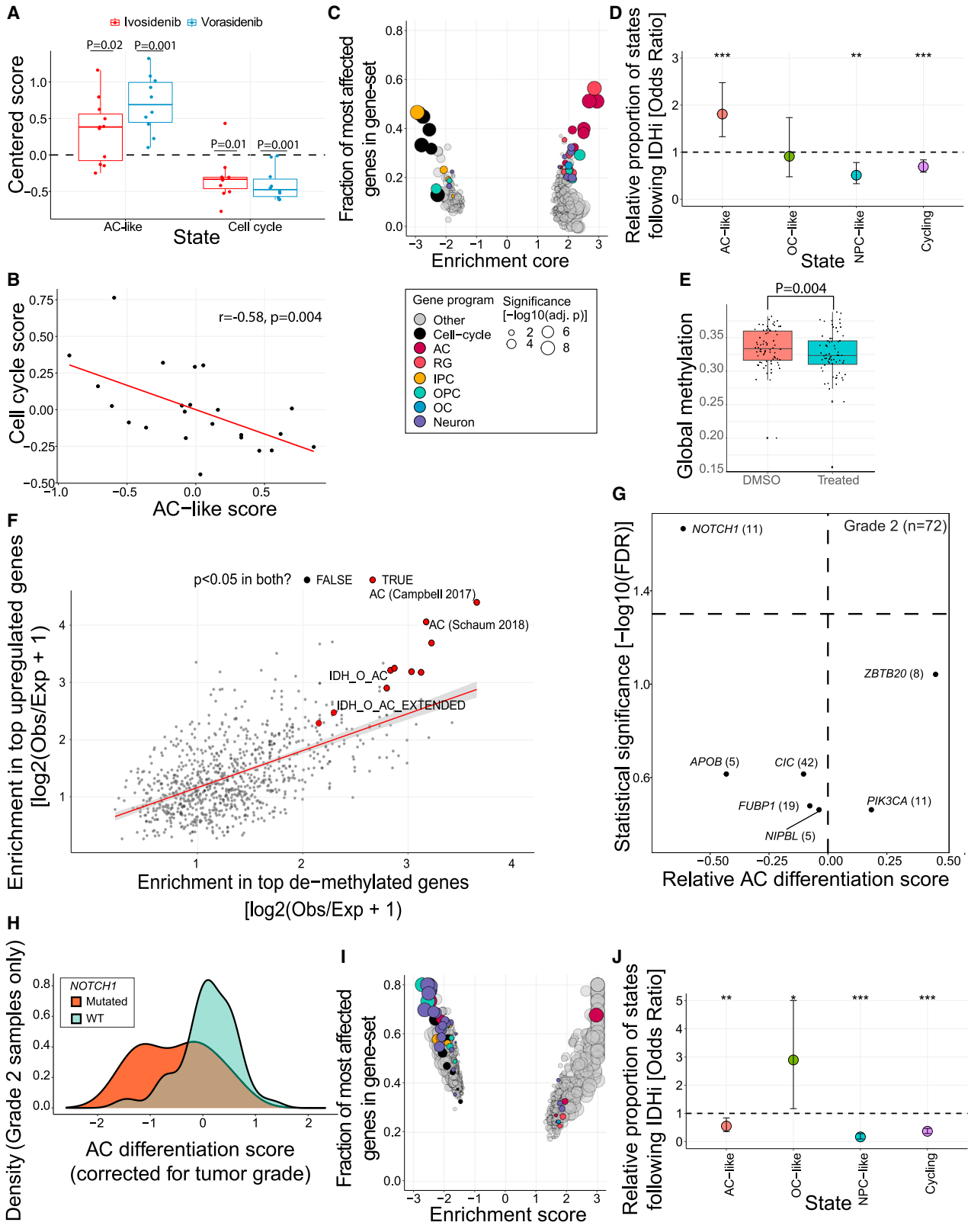

Figure 4. Validation and putative predictors of AC-like differentiation

(A) Distribution of AC-like and cell cycle scores across 21 IDHi-treated oligodendroglioma bulk RNA-seq profiles from a perioperative phase 1 trial (NCT03343197). Samples are grouped by pre-operative treatment condition. Scores are shown relative to the mean score of the two pre-operatively untreated

(legend continued on next page)

Please cite this article in press as: Spitzer et al., Mutant IDH inhibitors induce lineage differentiation in IDH-mutant oligodendroglioma, Cancer Cell (2024), https://doi.org/10.1016/j.ccell.2024.03.008

only observed in the context of AG-881 treatment, suggesting that *Notch1* is required for upregulation of AC-related genes (i.e., AC-like differentiation) but not for their baseline expression.

DISCUSSION

Our study provides a proof-of-concept for targeted differentiation therapy with mutant IDH inhibitors directly in patients with IDH-mutant glioma. While differentiation of malignant cells in patients treated with IDHi has been observed in acute myeloid leukemia (AML),[36] this, to our knowledge, had not been demonstrated in glioma. It is important to clarify here that this "differentiation effect" does not mean that malignant cells go through complete differentiation making them comparable to non-malignant glial cells. Rather, the malignant cells transcriptionally activate an expression program of dozens of genes that is similar, but not identical, to a differentiation program of normal glial cells, and the activation of this transcriptional program is inversely related to the proliferative capacity of cells, as demonstrated previously[21] and in this work. Thus, malignant cells with a "differentiated" transcriptional program remain malignant cells that are distinct from normal glial cells; but, importantly, they become less proliferative and less "stem-like" and hence are expected to be associated with slower disease progression.

Our study has three main limitations. First, our single cell on-treatment analysis includes only three oligodendroglioma patients that derived clinical benefit from IDHi and four astrocytoma patients that progressed while on treatment, reflecting the extreme complexity of obtaining on-treatment glioma tissue. These two cohorts cannot be directly compared due to differences between these glioma subtypes, and instead we compare each of them to subtype-matched untreated patients. We mitigated the limitation of cohort sizes by bulk analysis of 23 additional patient samples from a phase 1 trial and 134 untreated patient samples from TCGA. Nevertheless, future work would be needed to establish the generality of our findings across larger cohorts. Second, low-grade IDH-mutant glioma is notoriously difficult to model, restricting our ability to perform mechanistic studies. We partially mitigated this limitation by leveraging a recently developed mouse model of IDH-mutant glioma[31] that recapitulated our main results. Third, we defined patients as responsive to IDHi based on radiographic stable disease, yet the significance of stable disease in the context of slowly progressing tumors is difficult to ascertain. However, it is important to note that NCT04164901[17] supported the use of radiographic stable disease as a clinical endpoint in the context of IDHi. Moreover, all three patients in our cohort have remained stable on IDHi for more than 5 years, strongly supporting their status as responders.

In summary, we leveraged three types of data—a small single cell/nuclei-RNAseq cohort, large bulk RNA-seq cohorts, and an *in vitro* model. While each of these approaches has its own limitations, all three demonstrate increased AC-like and decreased cell cycle expression on IDHi, thus converging to the same conclusion—that treatment with an IDH inhibitor in the context of a low grade 1p/19q-codeleted IDH-mutant glioma induces the glioma cells to differentiate toward an AC-like phenotype while becoming less proliferative. This understanding of IDHi response may help to (1) identify those patients who are more likely to benefit from it, (2) assess response and resistance to differentiation therapy in low-grade gliomas, and (3) aid the identification of potential targets for combination strategies.

STAR★METHODS

Detailed methods are provided in the online version of this paper and include the following:

- KEY RESOURCES TABLE

samples. p values were computed for each treatment group separately using a one-sided t test with the alternative hypothesis that the mean is greater or lesser than zero for the AC-like and cell cycle scores, respectively. Throughout this figure the boxplots reflect the following summary statistics. (1) The line splitting the box represents the median value. (2) The lower and upper edges correspond to the first and third quartiles (the 25th and 75th percentiles). (3) The upper whisker extends from the edge to the largest value no further than 1.5 * IQR from the edge. (4) The lower whisker extends from the edge to the smallest value at most 1.5 * IQR of the edge. (5) Data beyond the end of the whiskers are plotted individually as outlying points.

(B) Association between AC-like and cell cycle scores across n = 23 (n = 21 treated) bulk RNA-seq oligodendroglioma samples. Trend line was computed using linear regression.

(C) Comparison of IDHi-treated and untreated *Notch1*-WT mouse *Idh1*$^{LSL\text{-}R132H}$;*Trp53*$^{flox/flox}$;*Olig2*^{Cre} glioma cells using GSEA, similar to the analysis shown in Figure 3A.

(D) Comparison of the proportion of cells assigned to each state in the IDHi-treated and untreated *Notch1*-WT mouse *Idh1*$^{LSL\text{-}R132H}$;*Trp53*$^{flox/flox}$;*Olig2*^{Cre} glioma cells. Odds ratio, confidence interval and p value were derived from Fisher's test. OR > 1 reflects increased proportions of the particular cell state in the IDHi-treated relative to the untreated cells. Significance levels: *p < 0.05, **p < 0.01, ***p < 0.001.

(E) Global methylation in IDHi-treated vs. untreated mouse *Idh1*$^{LSL\text{-}R132H}$;*Trp53*$^{flox/flox}$;*Olig2*^{Cre} glioma cells. Each dot represents a cell. p value was computed using a one-sided Kolmogorov-Smirnov test.

(F) Shown are 905 gene-sets that have an overlap greater than 0 with both 100 most demethylated and 100 most upregulated genes (i.e., observed overlap). The expected overlap is the overlap between each gene-set and the genes that passed QC in methylation and expression data independently. Red dots represent gene-sets that are significantly enriched (with a p value <0.05, one-sided Fisher's test) in both methylation and expression data. Trend line was computed using linear regression.

(G) Analysis of the association between recurrent mutations (in at least five tumors) and AC-like differentiation scores, for oligodendroglioma tumors of grade 2 (left) and of grade 3 (right) reveals a significant association (FDR-adjusted p value = 0.02, Wilcoxon rank-sum test) between mutations in *NOTCH1* and low degree of AC-like differentiation in grade 2 lesions (11/72 samples) but not in grade 3 lesions (16/62 samples). Each panel shows the difference in average AC-like differentiation score between tumors with and those without a specific mutation (X axis), and the significance of that score (Y axis, defined by -log10 of the p value calculated by t test and corrected for multiple testing by the Benjamini-Hochberg method). Horizontal line shows a significance threshold (FDR = 0.05), highlighting *NOTCH1* in grade 2 oligodendroglioma as the only significant association; Vertical line represents the mean AC-like differentiation score.

(H) Density of AC-like differentiation scores among grade 2 oligodendrogliomas with wild-type (green) or mutant (orange) *NOTCH1*.

(I and J) Similar analysis to that shown in (C and D) for the *Notch1*-KO mouse *Idh1*$^{LSL\text{-}R132H}$;*Trp53*$^{flox/flox}$;*Olig2*^{Cre} glioma cells.

See also Figure S5 and Tables S4 and S5.

SUPPLEMENTAL INFORMATION

Supplemental information can be found online at https://doi.org/10.1016/j.ccell.2024.03.008.

ACKNOWLEDGMENTS

This work was supported by NIH-NCI R01CA276765 (M.L.S. and D.P.C.), R37CA245523 (M.L.S), P50CA165962 (D.P.C., K.L.L., and M.L.S.), R01CA188228 (K.L.L.), R01CA258763 (M.L.S. and D.A.L.), U19CA264504 (M.L.S. and K.L.L) and an ERC (European Research Council) consolidator grant (I.T.). It was also supported by a Broad Institute–Israel Science Foundation Collaborative Project Award (I.T. and M.L.S.), the MGH Research Scholars Award (M.L.S.), grants from the Mark Foundation Emerging Leader Award (M.L.S.) and 3000 Miles to the Cure (K.L.L.). I.T. is the incumbent of the Dr. Celia Zwillenberg-Fridman and Dr. Lutz Zwillenberg Career Development Chair, and is supported by the Zuckerman STEM Leadership Program, the Mexican Friends New Generation, the Benoziyo Endowment Fund and grants from the Human Frontiers Science Program. A.S. is partially supported by the Israeli Council for Higher Education (CHE) via the Weizmann Data Science Research Center. We acknowledge C. Carpentier and A. Dridi-Aloulou for preparation and processing of samples; L. Liang and the OncoNeurotek tumor bank for sharing samples.

AUTHOR CONTRIBUTIONS

A.S., S.G., D.P.C., M.L.S., and I.T. conceived the project, designed the study, and interpreted results. MN provided expertise critical for the revision. S.G. and H.R.W. collected oligodendroglioma single cells and generated sequencing data. M.N. and A.J. performed single-cell library preparation for glioma models A.S., R.C.-M., and I.T. performed computational analyses. J.M.F., R.L.S., and R.M. provided flow cytometry expertise. L.N.G.C., D.P.C., J.J.M, I.A.-R., M.T., M.S., P.Y.W., W.P., and K.L.L. identified and consented patients for the study. M.N performed single-cell multi-omics data generation (DNAme+RNA). R.R. and D.A.L. provided expertise for multi-omic (DNAme+RNA) single-cell genomics. J.J.Y.L, C.K.L., H.N., H.W., and D.N.L. provided experimental and analytical support. J.F. designed and performed the *Notch1* CRISPR-KD experiment. I.T. and M.L.S. jointly supervised this work and interpreted results. A.S., S.G., M.N., K.L.L, D.P.C., M.L.S., and I.T. wrote the manuscript with feedback from all authors.

DECLARATION OF INTERESTS

M.L.S. is equity holders, scientific co-founder and advisory board member of Immunitas Therapeutics. I.T. is advisory board member of Immunitas Therapeutics. D.P.C. has consulted for Lilly, Incephalo, Boston Pharmaceuticals, Servier, Boston Scientific and Pyramid Biosciences (equity interest), and has received honoraria and travel reimbursement from Merck for invited lectures. J.J.M. received consulting fees from Servier. The authors declare that such activities have no relationship to the present study. M.T. reports consulting or advisory role for Servier, Novocure, Resilience, Agios Pharmaceutical, Integragen, and Taiho Oncology, honoraria for Ono, and research funding from Sanofi. P.Y.W. reports research support from Astra Zeneca, Black Diamond, Bristol Meyers Squibb, Chimerix, Eli Lily, Erasca, Global Coalition For Adaptive Research, Kazia, MediciNova, Merck, Novartis, Quadriga, Servier, VBI Vaccines and consulting or advisory role for Anheart, Astra Zeneca, Black Diamond, Celularity, Chimerix, Day One Bio, Genenta, Glaxo Smith Kline, Kintara, Merck, Mundipharma, Novartis, Novocure, Prelude Therapeutics, Sagimet, Sapience, Servier, Symbio, Tango, Telix, VBI Vaccines. K.L.L is equity holder, consultant, and co-founder of Travera, is a consultant for BMS, Blaze Biosciences and Integragen, and has grant research funding through DFCI from BMS and Lilly. L.N.G.C. has received research support from Merck & Co, and consulting fees from BMJ Best Practice and Oakstone Publishing.

Received: February 2, 2023
Revised: January 5, 2024
Accepted: March 13, 2024
Published: April 4, 2024

REFERENCES

1. Parsons, D.W., Jones, S., Zhang, X., Lin, J.C.H., Leary, R.J., Angenendt, P., Mankoo, P., Carter, H., Siu, I.M., Gallia, G.L., et al. (2008). An integrated genomic analysis of human glioblastoma multiforme. Science *321*, 1807–1812. https://doi.org/10.1126/science.1164382.
2. Yan, H., Parsons, D.W., Jin, G., McLendon, R., Rasheed, B.A., Yuan, W., Kos, I., Batinic-Haberle, I., Jones, S., Riggins, G.J., et al. (2009). IDH1 and IDH2 Mutations in Gliomas. N. Engl. J. Med. *360*, 765–773. https://doi.org/10.1056/NEJMoa0808710.

3. Borger, D.R., Tanabe, K.K., Fan, K.C., Lopez, H.U., Fantin, V.R., Straley, K.S., Schenkein, D.P., Hezel, A.F., Ancukiewicz, M., Liebman, H.M., et al. (2012). Frequent Mutation of Isocitrate Dehydrogenase (IDH)1 and IDH2 in Cholangiocarcinoma Identified Through Broad Based Tumor Genotyping. Oncol. *17*, 72–79. https://doi.org/10.1634/theoncologist.2011-0386.

4. Mardis, E.R., Ding, L., Dooling, D.J., Larson, D.E., McLellan, M.D., Chen, K., Koboldt, D.C., Fulton, R.S., Delehaunty, K.D., McGrath, S.D., et al. (2009). Recurring Mutations Found by Sequencing an Acute Myeloid Leukemia Genome. N. Engl. J. Med. *361*, 1058–1066. https://doi.org/10.1056/NEJMoa0903840.

5. Ward, P.S., Patel, J., Wise, D.R., Abdel-Wahab, O., Bennett, B.D., Coller, H.A., Cross, J.R., Fantin, V.R., Hedvat, C.V., Perl, A.E., et al. (2010). The Common Feature of Leukemia-Associated IDH1 and IDH2 Mutations Is a Neomorphic Enzyme Activity Converting α-Ketoglutarate to 2-Hydroxyglutarate. Cancer Cell *17*, 225–234. https://doi.org/10.1016/j.ccr.2010.01.020.

6. Gross, S., Cairns, R.A., Minden, M.D., Driggers, E.M., Bittinger, M.A., Jang, H.G., Sasaki, M., Jin, S., Schenkein, D.P., Su, S.M., et al. (2010). Cancer-associated metabolite 2-hydroxyglutarate accumulates in acute myelogenous leukemia with isocitrate dehydrogenase 1 and 2 mutations. J. Exp. Med. *207*, 339–344. https://doi.org/10.1084/jem.20092506.

7. Chowdhury, R., Yeoh, K.K., Tian, Y.M., Hillringhaus, L., Bagg, E.A., Rose, N.R., Leung, I.K.H., Li, X.S., Woon, E.C.Y., Yang, M., et al. (2011). The oncometabolite 2 hydroxyglutarate inhibits histone lysine demethylases. EMBO Rep. *12*, 463–469. https://doi.org/10.1038/embor.2011.43.

8. Xu, W., Yang, H., Liu, Y., Yang, Y., Wang, P., Kim, S.H., Ito, S., Yang, C., Wang, P., Xiao, M.T., et al. (2011). Oncometabolite 2-hydroxyglutarate is a competitive inhibitor of α-ketoglutarate-dependent dioxygenases. Cancer Cell *19*, 17–30. https://doi.org/10.1016/j.ccr.2010.12.014.

9. Flavahan, W.A., Drier, Y., Liau, B.B., Gillespie, S.M., Venteicher, A.S., Stemmer-Rachamimov, A.O., Suvà, M.L., and Bernstein, B.E. (2016). Insulator dysfunction and oncogene activation in IDH mutant gliomas. Nature *529*, 110–114. https://doi.org/10.1038/nature16490.

10. Lu, C., Ward, P.S., Kapoor, G.S., Rohle, D., Turcan, S., Abdel-Wahab, O., Edwards, C.R., Khanin, R., Figueroa, M.E., Melnick, A., et al. (2012). IDH mutation impairs histone demethylation and results in a block to cell differentiation. Nature *483*, 474–478. https://doi.org/10.1038/nature10860.

11. Noushmehr, H., Weisenberger, D.J., Diefes, K., Phillips, H.S., Pujara, K., Berman, B.P., Pan, F., Pelloski, C.E., Sulman, E.P., Bhat, K.P., et al. (2010). Identification of a CpG Island Methylator Phenotype that Defines a Distinct Subgroup of Glioma. Cancer Cell *17*, 510–522. https://doi.org/10.1016/j.ccr.2010.03.017.

12. Turcan, S., Rohle, D., Goenka, A., Walsh, L.A., Fang, F., Yilmaz, E., Campos, C., Fabius, A.W.M., Lu, C., Ward, P.S., et al. (2012). IDH1 mutation is sufficient to establish the glioma hypermethylator phenotype. Nature *483*, 479–483. https://doi.org/10.1038/nature10866.

13. Tateishi, K., Wakimoto, H., Iafrate, A.J., Tanaka, S., Loebel, F., Lelic, N., Wiederschain, D., Bedel, O., Deng, G., Zhang, B., et al. (2015). Extreme Vulnerability of IDH1 Mutant Cancers to NAD+ Depletion. Cancer Cell *28*, 773–784. https://doi.org/10.1016/j.ccell.2015.11.006.

14. Kopinja, J., Sevilla, R.S., Levitan, D., Dai, D., Vanko, A., Spooner, E., Ware, C., Forget, R., Hu, K., Kral, A., et al. (2017). A Brain Penetrant Mutant IDH1 Inhibitor Provides in Vivo Survival Benefit. Sci. Rep. *7*, 13853. https://doi.org/10.1038/s41598-017-14065-w.

15. Pusch, S., Krausert, S., Fischer, V., Balss, J., Ott, M., Schrimpf, D., Capper, D., Sahm, F., Eisel, J., Beck, A.C., et al. (2017). Pan-mutant IDH1 inhibitor BAY 1436032 for effective treatment of IDH1 mutant astrocytoma *in vivo*. Acta Neuropathol. *133*, 629–644. https://doi.org/10.1007/s00401-017-1677-y.

16. Rohle, D., Popovici-Muller, J., Palaskas, N., Turcan, S., Grommes, C., Campos, C., Tsoi, J., Clark, O., Oldrini, B., Komisopoulou, E., et al. (2013). An inhibitor of mutant IDH1 delays growth and promotes differentiation of glioma cells. Science *340*, 626–630. https://doi.org/10.1126/science.1236062.

17. Mellinghoff, I.K., van den Bent, M.J., Blumenthal, D.T., Touat, M., Peters, K.B., Clarke, J., Mendez, J., Yust-Katz, S., Welsh, L., Mason, W.P., et al. (2023). Vorasidenib in IDH1- or IDH2-Mutant Low-Grade Glioma. N. Engl. J. Med. *389*, 589–601. https://doi.org/10.1056/NEJMOA2304194.

18. Mellinghoff, I.K., Ellingson, B.M., Touat, M., Maher, E., De La Fuente, M.I., Holdhoff, M., Cote, G.M., Burris, H., Janku, F., Young, R.J., et al. (2020). Ivosidenib in Isocitrate Dehydrogenase 1 – Mutated Advanced Glioma. J. Clin. Oncol. *38*, 3398–3406. https://doi.org/10.1200/jco.19.03327.

19. Picelli, S., Faridani, O.R., Björklund, A.K., Winberg, G., Sagasser, S., and Sandberg, R. (2014). Full-length RNA-seq from single cells using Smart-seq2. Nat. Protoc. *9*, 171–181. https://doi.org/10.1038/nprot.2014.006.

20. Tirosh, I., Venteicher, A.S., Hebert, C., Escalante, L.E., Patel, A.P., Yizhak, K., Fisher, J.M., Rodman, C., Mount, C., Filbin, M.G., et al. (2016). Single-cell RNA-seq supports a developmental hierarchy in human oligodendroglioma. Nature *539*, 309–313. https://doi.org/10.1038/nature20123.

21. Venteicher, A.S., Tirosh, I., Hebert, C., Yizhak, K., Neftel, C., Filbin, M.G., Hovestadt, V., Escalante, L.E., Shaw, M.L., Rodman, C., et al. (2017). Decoupling genetics, lineages, and microenvironment in IDH-mutant gliomas by single-cell RNA-seq. Science *355*, eaai8478. https://doi.org/10.1126/science.aai8478.

22. Velmeshev, D., Schirmer, L., Jung, D., Haeussler, M., Perez, Y., Mayer, S., Bhaduri, A., Goyal, N., Rowitch, D.H., and Kriegstein, A.R. (2019). Single-cell genomics identifies cell type–specific molecular changes in autism. Science *364*, 685–689. https://doi.org/10.1126/science.aav8130.

23. Tabula Muris Consortium, Overall coordination, Logistical coordination, Organ collection and processing, Library preparation and sequencing, Computational data analysis, Cell type annotation, Writing group, Supplemental text writing group, Principal investigators, et al. (2018). Single-cell transcriptomics of 20 mouse organs creates a Tabula Muris. Nature *562*, 367–372. https://doi.org/10.1038/s41586-018-0590-4.

24. Campbell, J.N., Macosko, E.Z., Fenselau, H., Pers, T.H., Lyubetskaya, A., Tenen, D., Goldman, M., Verstegen, A.M.J., Resch, J.M., McCarroll, S.A., et al. (2017). A molecular census of arcuate hypothalamus and median eminence cell types. Nat. Neurosci. *20*, 484–496. https://doi.org/10.1038/nn.4495.

25. Habib, N., Li, Y., Heidenreich, M., Swiech, L., Avraham-Davidi, I., Trombetta, J.J., Hession, C., Zhang, F., and Regev, A. (2016). Div-Seq: Single-nucleus RNA-Seq reveals dynamics of rare adult newborn neurons. Science *353*, 925–928. https://doi.org/10.1126/science.aad7038.

26. Polioudakis, D., de la Torre-Ubieta, L., Langerman, J., Elkins, A.G., Shi, X., Stein, J.L., Vuong, C.K., Nichterwitz, S., Gevorgian, M., Opland, C.K., et al. (2019). A Single-Cell Transcriptomic Atlas of Human Neocortical Development during Mid-gestation. Neuron *103*, 785–801.e8. https://doi.org/10.1016/j.neuron.2019.06.011.

27. Nowakowski, T.J., Bhaduri, A., Pollen, A.A., Alvarado, B., Mostajo-Radji, M.A., Di Lullo, E., Haeussler, M., Sandoval-Espinosa, C., Liu, S.J., Velmeshev, D., et al. (2017). Spatiotemporal gene expression trajectories reveal developmental hierarchies of the human cortex. Science *358*, 1318–1323. https://doi.org/10.1126/science.aap8809.

28. Neftel, C., Laffy, J., Filbin, M.G., Hara, T., Shore, M.E., Rahme, G.J., Richman, A.R., Silverbush, D., Shaw, M.L., Hebert, C.M., et al. (2019). An Integrative Model of Cellular States, Plasticity, and Genetics for Glioblastoma. Cell *178*, 835–849.e21. https://doi.org/10.1016/j.cell.2019.06.024.

29. Nduom, E.K., Gephart, M.H., Chheda, M.G., Suva, M.L., Amankulor, N., Battiste, J.D., Campian, J.L., Dacey, R.G., Das, S., Fecci, P.E., et al. (2021). Re-evaluating Biopsy for Recurrent Glioblastoma: A Position Statement by the Christopher Davidson Forum Investigators. Neurosurgery *89*, 129–132. https://doi.org/10.1093/NEUROS/NYAB063.

30. Mellinghoff, I.K., Lu, M., Wen, P.Y., Taylor, J.W., Maher, E.A., Arrillaga-Romany, I., Peters, K.B., Ellingson, B.M., Rosenblum, M.K., Chun, S., et al. (2023). Vorasidenib and ivosidenib in IDH1-mutant low-grade glioma: a randomized, perioperative phase 1 trial. Nat. Med. *29*, 615–622. https://doi.org/10.1038/s41591-022-02141-2.

31. Laugesen, E., Tian, R., Wu, A., El Ghamrasni, S., Levine, A., Aamir, Z., Nobre, L.F., Petrecca, K., McBrayer, S., Suva, M., et al. (2023). MODL-47. A NEW MOUSE MODEL OF IDH MUTATED GLIOMAS IDENTIFIES TUMOR CELLS OF ORIGIN AND DETERMINANTS OF SENSITIVITY TO IDH INHIBITORS. Neuro Oncol. *25*, v309. https://doi.org/10.1093/NEUONC/NOAD179.1198.

32. Gu, H., Raman, A.T., Wang, X., Gaiti, F., Chaligne, R., Mohammad, A.W., Arczewska, A., Smith, Z.D., Landau, D.A., Aryee, M.J., et al. (2021). Smart-RRBS for single-cell methylome and transcriptome analysis. Nat. Protoc. *16*, 4004–4030. https://doi.org/10.1038/s41596-021-00571-9.

33. Chaligne, R., Suvà, M.L., Silverbush, D., Schiffman, J.S., Weisman, H.R., Kluegel, L., Gritsch, S., Deochand, S.D., Gonzalez Castro, L.N., Richman, A.R., et al. (2021). Epigenetic encoding, heritability and plasticity of glioma transcriptional cell states. Nat. Genet. *53*, 1469–1479. https://doi.org/10.1038/s41588-021-00927-7.

34. Modrek, A.S., Golub, D., Khan, T., Bready, D., Prado, J., Bowman, C., Deng, J., Zhang, G., Rocha, P.P., Raviram, R., et al. (2017). Low-Grade Astrocytoma Mutations in IDH1, P53, and ATRX Cooperate to Block Differentiation of Human Neural Stem Cells via Repression of SOX2. Cell Rep. *21*, 1267–1280. https://doi.org/10.1016/j.celrep.2017.10.009.

35. Johannessen, T.C.A., Mukherjee, J., Viswanath, P., Ohba, S., Ronen, S.M., Bjerkvig, R., and Pieper, R.O. (2016). Rapid conversion of mutant IDH1 from driver to passenger in a model of human gliomagenesis. Mol. Cancer Res. *14*, 976–983. https://doi.org/10.1158/1541-7786.MCR-16-0141.

36. Wang, F., Travins, J., DeLaBarre, B., Penard-Lacronique, V., Schalm, S., Hansen, E., Straley, K., Kernytsky, A., Liu, W., Gliser, C., et al. (2013). Targeted inhibition of mutant IDH2 in leukemia cells induces cellular differentiation. Science *340*, 622–626. https://doi.org/10.1126/science.1234769.

37. Lemonnier, F., Cairns, R.A., Inoue, S., Li, W.Y., Dupuy, A., Broutin, S., Martin, N., Fataccioli, V., Pelletier, R., Wakeham, A., et al. (2016). The IDH2 R172K mutation associated with angioimmunoblastic T-cell lymphoma produces 2HG in T cells and impacts lymphoid development. Proc. Natl. Acad. Sci. USA *113*, 15084–15089. https://doi.org/10.1073/pnas.1617929114.

38. Jonkers, J., Meuwissen, R., van der Gulden, H., Peterse, H., van der Valk, M., and Berns, A. (2001). Synergistic tumor suppressor activity of BRCA2 and p53 in a conditional mouse model for breast cancer. Nat. Genet. *29*, 418–425. https://doi.org/10.1038/ng747.

39. Zawadzka, M., Rivers, L.E., Fancy, S.P.J., Zhao, C., Tripathi, R., Jamen, F., Young, K., Goncharevich, A., Pohl, H., Rizzi, M., et al. (2010). CNS-resident glial progenitor/stem cells produce Schwann cells as well as oligodendrocytes during repair of CNS demyelination. Cell Stem Cell *6*, 578–590. https://doi.org/10.1016/j.stem.2010.04.002.

40. Fortin, J., Tian, R., Zarrabi, I., Hill, G., Williams, E., Sanchez-Duffhues, G., Thorikay, M., Ramachandran, P., Siddaway, R., Wong, J.F., et al. (2020). Mutant ACVR1 Arrests Glial Cell Differentiation to Drive Tumorigenesis in Pediatric Gliomas. Cancer Cell *37*, 308–323.e12. https://doi.org/10.1016/J.CCELL.2020.02.002.

41. Patel, A.P., Tirosh, I., Trombetta, J.J., Shalek, A.K., Gillespie, S.M., Wakimoto, H., Cahill, D.P., Nahed, B.V., Curry, W.T., Martuza, R.L., et al. (2014). Single-cell RNA-seq highlights intratumoral heterogeneity in primary glioblastoma. Science *344*, 1396–1401. https://doi.org/10.1126/science.1254257.

42. Filbin, M.G., Tirosh, I., Hovestadt, V., Shaw, M.L., Escalante, L.E., Mathewson, N.D., Neftel, C., Frank, N., Pelton, K., Hebert, C.M., et al. (2018). Developmental and oncogenic programs in H3K27M gliomas dissected by single-cell RNA-seq. Science *360*, 331–335. https://doi.org/10.1126/science.aao4750.

43. Langmead, B., Trapnell, C., Pop, M., and Salzberg, S.L. (2009). Ultrafast and memory-efficient alignment of short DNA sequences to the human genome. Genome Biol. *10*, R25. https://doi.org/10.1186/gb-2009-10-3-r25.

44. Li, B., and Dewey, C.N. (2011). RSEM: Accurate transcript quantification from RNA-Seq data with or without a reference genome. BMC Bioinf. *12*, 323. https://doi.org/10.1186/1471-2105-12-323.

45. Subramanian, A., Tamayo, P., Mootha, V.K., Mukherjee, S., Ebert, B.L., Gillette, M.A., Paulovich, A., Pomeroy, S.L., Golub, T.R., Lander, E.S., and Mesirov, J.P. (2005). Gene set enrichment analysis: A knowledge-based approach for interpreting genome-wide expression profiles. Proc. Natl. Acad. Sci. USA *102*, 15545–15550. https://doi.org/10.1073/PNAS.0506580102.

46. Mootha, V.K., Lindgren, C.M., Eriksson, K.-F., Subramanian, A., Sihag, S., Lehar, J., Puigserver, P., Carlsson, E., Ridderstråle, M., Laurila, E., et al. (2003). PGC-1α-responsive genes involved in oxidative phosphorylation are coordinately downregulated in human diabetes. Nat. Genet. *343*, 267–273. https://doi.org/10.1038/ng1180.

47. Korotkevich, G., Sukhov, V., Budin, N., Shpak, B., Artyomov, M.N., and Sergushichev, A. (2021). Fast gene set enrichment analysis. Preprint at bioRxiv. https://doi.org/10.1101/060012.

48. Hao, Y., Hao, S., Andersen-Nissen, E., Mauck, W.M., Zheng, S., Butler, A., Lee, M.J., Wilk, A.J., Darby, C., Zager, M., et al. (2021). Integrated analysis of multimodal single-cell data. Cell *184*, 3573–3587.e29. https://doi.org/10.1016/J.CELL.2021.04.048.

49. Colaprico, A., Silva, T.C., Olsen, C., Garofano, L., Cava, C., Garolini, D., Sabedot, T.S., Malta, T.M., Pagnotta, S.M., Castiglioni, I., et al. (2016). TCGAbiolinks: An R/Bioconductor package for integrative analysis of TCGA data. Nucleic Acids Res. *44*, e71. https://doi.org/10.1093/nar/gkv1507.

Please cite this article in press as: Spitzer et al., Mutant IDH inhibitors induce lineage differentiation in IDH-mutant oligodendroglioma, Cancer Cell (2024), https://doi.org/10.1016/j.ccell.2024.03.008

STAR★METHODS

KEY RESOURCES TABLE

REAGENT or RESOURCE	SOURCE	IDENTIFIER
Antibodies		
Anti-human CD45-VioBlue, (clone REA747)	Miltenyi Biotec	Cat# 130-110-775; RRID: AB_2658242
Anti-human CD3-PE, (clone BW264/56)	Miltenyi Biotec	Cat# 130-113-691; RRID: AB_2726232
Bacterial and virus strains		
None to report		
Biological samples		
Fresh glioma specimens were obtained following informed consent for IRB approved studies	Brigham and Women's Hospital/Dana-Farber Cancer Institute, Massachusetts General Hospital, Hôpitaux Universitaires La Pitié Salpêtrière	IRB# DF/HCC 10-417, AC-2013-1962
Chemicals, peptides, and recombinant proteins		
Buffer TCL	Qiagen	Cat# 1031576 RRID: N/A
Bovine Serum Albumin	Sigma Aldrich	Cat# A3059 RRID: N/A
Calcein, AM, cell-permeant dye	Invitrogen	Cat# C3100MP RRID: N/A
TO-PRO-3 Iodide	Invitrogen	Cat# T3605 RRID: N/A
Maxima H Minus Reverse Transcriptase	Thermo Scientific	Cat# EP0753 RRID: N/A
KAPA HiFi HotStart ReadyMix	Roche	Cat# KK2602 RRID: N/A
dNTP Mix (10 mM each)	Thermo Scientific	Cat# R0192 RRID: N/A
Recombinant RNase Inhibitor	Takara	Cat# 2313B RRID: N/A
D-(+)-Trehalose Solution, 1M	LifeSciences	Cat# TS1M-100 RRID: N/A
Magnesium chloride 1M	Invitrogen	Cat# AM9530G RRID: N/A
RNAscope Hydrogen Peroxide	ACDbio	Cat# 322335 RRID: N/A
RNAscope Target Retrieval Reagent	ACDbio	Cat# 322000 RRID: N/A
RNAscope Protease Plus	ACDbio	Cat# 322331 RRID: N/A
2-Mercaptoethanol	Sigma-Aldrich	Cat# M6250 RRID: N/A
VECTASHIELD Antifade Mounting Medium	Vectorlabs	Cat# H-1000 RRID: AB_2336789
NaCl (5 M), RNase-free	Thermo Fisher Scientific	Cat# AM9759 RRID: N/A
UltraPure 1 M Tris-HCl Buffer, pH 7.5	Thermo Fisher Scientific	Cat# 15567027 RRID: N/A
Calcium chloride solution	Sigma Aldrich	Cat# 21115 RRID: N/A

(*Continued on next page*)

Please cite this article in press as: Spitzer et al., Mutant IDH inhibitors induce lineage differentiation in IDH-mutant oligodendroglioma, Cancer Cell (2024), https://doi.org/10.1016/j.ccell.2024.03.008

Continued

REAGENT or RESOURCE	SOURCE	IDENTIFIER
Magnesium chloride solution	Sigma Aldrich	Cat# M1028 RRID: N/A
CHAPS Detergent	Thermo Fisher Scientific	Cat# 28300 RRID: N/A
Proteinase K	New England Biolabs	Cat# P8107S RRID: N/A
CutSmart buffer, 10×	New England Biolabs	Cat# P7204S RRID: N/A
MspI	New England Biolabs	Cat# R0106L RRID: N/A
Kenow fragment	New England Biolabs	Cat# M0212L RRID: N/A
Deoxynucleotide solution set	New England Biolabs	Cat# N0447L RRID: N/A
T4 DNA ligase	New England Biolabs	Cat# M0202M RRID: N/A
ATP solution, 100mM	Thermo Fisher Scientific	Cat# R0441 RRID: N/A
2× KAPA HiFi HotStart Uracil^{+} ReadyMix	Roche	Cat# KK2802 RRID: N/A
PEG 8000	Millipore Sigma	Cat# 25322-68-3 RRID: N/A
Tween20	Thermo Fisher Scientific	Cat# AAJ20605AP RRID: N/A
DTT	Thermo Fisher Scientific	Cat# 707256ML RRID: N/A
Vorasidenib	MedChemExpress	Cat #HY-104042
TSM Base medium	Wisent	Cat #305-485-CL
B-27 supplement without vitamin A	Thermo Fisher	Cat #12587-010
Recombinant H-EGF	Shenandoah Biotech	Cat #100-26
Recombinant H-FGF-basic-154	Shenandoah Biotech	Cat #100-146
Recombinant H-PDGF-AA	Shenandoah Biotech	Cat #100-16
Recombinant H-PDGF-BB	Shenandoah Biotech	Cat #100-28
Critical commercial assays		
Brain Tumor Dissociation Kit (P)	Miltenyi	Cat# 130-095-942 RRID: N/A
Agencourt RNAClean XP	Beckman Coulter	Cat# A66514 RRID: N/A
Agencourt AMPure XP	Beckman Coulter	Cat# A63882 RRID: N/A
SPRIselect	Beckman Coulter	Cat# B233818 RRID: N/A
Nextera XT DNA Library Preparation Kit (96 samples)	Illumina	Cat# FC-131-1096 RRID: N/A
NextSeq 500/550 High Output Kit v2.5 (75 Cycles)	Illumina	Cat# 20024906 RRID: N/A
NextSeq 1000/2000 P2 reagent (100 Cycles)	Illumina	Cat# 20046681 RRID: N/A
Bioanalyzer High Sensitivity DNA Analysis	Agilent	Cat# 5067-4626 RRID: N/A
Qubit dsDNA HS Assay kit	Invitrogen	Cat# Q32854 RRID: N/A
RNAscope 2.5 HD Duplex Detection Kit	ACDbio	Cat# 322430 RRID: N/A

(*Continued on next page*)

Please cite this article in press as: Spitzer et al., Mutant IDH inhibitors induce lineage differentiation in IDH-mutant oligodendroglioma, Cancer Cell (2024), https://doi.org/10.1016/j.ccell.2024.03.008

Continued

REAGENT or RESOURCE	SOURCE	IDENTIFIER
Chromium GEM Single Cell 3' GEM, Library Kit v3.1	10X GENOMICS	Cat# 1000128 RRID: N/A
Chromium GEM Single Cell 3' Gel Bead Kit v3.1	10X GENOMICS	Cat# 1000128 RRID: N/A
Chromium Next GEM Chip G Single Cell Kit	10X GENOMICS	Cat# 1000120 RRID: N/A
Chromium Single Cell 3'Feature Barcode Library Kit	10X GENOMICS	Cat# 1000079 RRID: N/A
EpiTect fast DNA bisulfite kit	Qiagen	Cat# 59824 RRID:N/A
Deposited data		
RNA sequencing data	Mellinghoff et al.[30] *Nat Med* 2023	dbGAP Phs003148.v1.p1
Single-cell RNA sequencing (patient samples SS2)	Tirosh et al.[20] *Nature* 2016	GSE70630
Single-cell RNA sequencing (patient samples SS2)	Venteicher et al.[21] *Science* 2017	GSE89567
RNA sequencing data	TCGA LGG cohort	Downloaded via GDC
Single-cell RNA sequencing (patient samples SS2)	This study	GSE260997
Single-cell RNA sequencing (patient samples 10x)	This study	GSE260928
Single-cell RNA sequencing (*Idh1*$^{LSL\text{-}R132H/+}$; *Trp53*$^{flox/flox}$;*Olig2*$^{Cre/+}$ mouse cell line)	This study	GSE260928
Single-cell RNA sequencing (multi-omics)	This study	GSE260933
Single-cell RNA sequencing (multi-omics)	This study	GSE260997
Experimental models: Cell lines		
Idh1$^{LSL\text{-}R132H/+}$;*Trp53*$^{flox/flox}$;*Olig2*$^{Cre/+}$ mouse cell line	This study	N/A
Experimental models: Organisms/strains		
None to report		
Oligonucleotides		
Oligo(dT) Primer (5′–AAGCAGTGGTATCAACGCAG AGTACTTTTTTTTTTTTTTTTTTTTTTTTTTTTTTVN-3')	IDT	N/A
ISPCR Primer (5′-AAGCAGTGGTATCAACGCAGAGT-3′)	IDT	N/A
Oligo(dT)_multiomics Primer (5'-BiotinTEG-AAGC AGTGGTATCAACGCAGAGTACT30VN-3')	IDT	N/A
sgRNA: Notch1_exon3: AGTGCCGCTGCCCACCAGGG	Thermo Fisher	N/A
sgRNA: Notch1_exon5: TACATACCCGTCCACTCCGG	Thermo Fisher	N/A
sgRNA: ROSA26: CTCCAGTCTTTCTAGAAGAT	Thermo Fisher	N/A
Recombinant DNA		
Hs-ALDOC	ACDbio	Cat# 407031 RRID: N/A
Hs-GFAP	ACDbio	Cat# 311801-C2 RRID: N/A
Hs-SOX4	ACDbio	Cat# 469911 RRID: N/A
Hs-MKI67	ACDbio	Cat# 591771-C2 RRID: N/A
LentiCRISPRv2GFP	Addgene; Laboratory of Dr. David Feldser	82416
psPAX2	Addgene; Laboratory of Dr. Didier Trono	2260
pMD2.G	Addgene; Laboratory of Dr. Didier Trono	12259
Software and algorithms		
Code supporting this analysis	This study	https://github.com/dravishays/IDHi/

(*Continued on next page*)

Please cite this article in press as: Spitzer et al., Mutant IDH inhibitors induce lineage differentiation in IDH-mutant oligodendroglioma, Cancer Cell (2024), https://doi.org/10.1016/j.ccell.2024.03.008

Continued

REAGENT or RESOURCE	SOURCE	IDENTIFIER
Other		
Noyes Spring Scissors	Fine Science Tools	Cat# 15514-12 RRID: N/A
40 um cell strainer	Fisher Scientific	Cat# 22363547 RRID: N/A
35 um cell strainer	Falcon	Cat# 352235 RRID: N/A
C-Chip Hemocytometers	INCYTO	Cat# DHCN012 RRID: N/A
Zymo-Spin IC columns	Zymo Research	Cat# C1004-50 RRID: N/A

RESOURCE AVAILABILITY

Lead contact

Further information and requests for resources should be directed to and will be fulfilled by the lead contact, Itay Tirosh (itay.tirosh@weizmann.ac.il).

Materials availability

Unique reagents generated in this study are available with an MTA.

Data and code availability

Single-cell RNA-seq data is publicly available at GEO: GSE260997, GSE260928, GSE260933. Accession numbers are listed in the key resources table. Publicly available datasets used in this study are indicated in the key resources table.

All original code is publicly available at github. DOIs are listed in the key resources table.

Any additional information required to reanalyze the data reported in this paper is available from the lead contact upon request.

EXPERIMENTAL MODEL AND STUDY PARTICIPANT DETAILS

Patient samples

Patients at Massachusetts General Hospital (MGH) were consented preoperatively in all cases according to Institutional Review Board DF/HCC 10-417.

Patient MGH170 was diagnosed in 2016 with grade 2 oligodendroglioma, 1p19q co-deleted, and after 21 28-day cycles of everolimus suffered recurrence in 2018. Patient MGH229 was initially diagnosed in 1999 with grade 2 oligodendroglioma, 1p19q co-deleted, and after maximal safe resection showed progression to grade 3 oligodendroglioma in 2010. After re-resection and 12 28-day cycles of temozolomide he suffered recurrence in 2019. Patient BWH445 was diagnosed in 2003 with grade 2 oligodendroglioma, 1p19q co-deleted, and after tumor resection followed by 12 28-day cycles of temozolomide he suffered disease progression in 2012. After re-resection and additional 6 28-day cycles of temozolomide they suffered recurrence in 2018. Following recurrence all three patients were enrolled in a clinical trial investigating mutant IDH inhibitors in the treatment of recurrent, low-grade, IDH-mutant gliomas (NCT03343197). This study had 2HG concentration measured in on-treatment primary tumor tissue as the primary end point and all patients underwent tumor resection after 28 (+7) days of IDHi treatment (Mellinghof et al., 2023, Nature Medicine). Patient MGH170 remains clinically and radiographically stable (as of 12/5/2023) after 60 months on treatment (since 11/19/2018, ongoing). Patient MGH229 remains clinically and radiographically stable (as of 11/27/2023) after 55 months on treatment (since 4/16/2019, ongoing). Patient BWH 445 remains clinically and radiographically stable (as of 11/16/2023) after 66 months on treatment (since 5/15/2018, ongoing).

Patient MGH202 was initially diagnosed in 2008 with grade 2 astrocytoma, 1p retained, 19q loss, and after maximal safe resection and proton radiation therapy showed progression to grade 3 astrocytoma in 2017. After partial re-resection and 4 months of Vorasidenib treatment the patient suffered radiographic disease progression.

Patient BWH20 was diagnosed in 2017 with grade II astrocytoma, 1p19q non-codeleted. After initial near total resection, he suffered recurrence in 2020. After recurrence the patient was enrolled in a clinical trial of Vorasidenib in patients with residual or recurrent IDH-mutant grade 2 glioma (NCT04164901, INDIGO trial). The patient was randomized to the Vorasidenib arm and remained on treatment from 11/2020 until he suffered radiographic disease progression in 2/2021.

Patient BWH5033 was diagnosed in 1999 with grade II astrocytoma, 1p19q non-codeleted. After initial resection he underwent re-resection for tumor recurrence in 2/2002, followed by 6 weeks of radiation therapy. He suffered radiographic tumor progression in 10/2006 and underwent re-resection. He then suffered disease recurrence and completed 12 28-day cycles of temozolomide from 9/2010 until 7/2011. He suffered radiographic tumor progression in 6/2012 and completed additional 5 28-day cycles of

temozolomide. Brain MRI in 11/2012 showed radiographic progression and he received PCV chemotherapy, which was stopped after 4 cycles due to hematologic toxicity. He then suffered recurrence in 1/2016 and underwent re-resection. Subsequently, he was enrolled in a clinical trial of IDH inhibitor 305 (NCT02381886) and remained on treatment from 3/24/2016 until 1/10/2017 when he suffered radiographic disease progression.

Patient PARIS was diagnosed in 2007 with grade II astrocytoma, 1p19q non-codeleted. After initial tumor resection, he suffered disease recurrence in 2012 and underwent re-resection. Subsequently, he was treated with Ivosidenib from 12/2015 until 2/2016 when he suffered radiographic disease progression. Re-resection after tumor progression revealed astrocytoma WHO grade IV.

Cell lines

Idh^{R132H} mouse glioma cells were generated from a forebrain tumor isolated from a *Idh1*$^{LSL\text{-}R132H}$;*Trp53*$^{flox/flox}$;*Olig2*^{Cre} mouse.[31,37–39] This genetically engineered mouse model develops diffuse gliomas with full penetrance. Tumors were isolated and cell lines established as described previously.[40] Cells could be propagated for at least 20 passages while maintaining R-2-HG production, which could be fully suppressed with 1 μM AG-881 (Vorasidenib). *Notch1*-targeting sgRNAs targeting exon 3 and exon 5, in the region coding for the first stretch of EGF-like repeats, were cloned in in LentiCRISPRv2GFP (obtained from Addgene, from the laboratory of David Feldser). Procedures for CRISPR lentivirus production, cell transduction, culture, RNA isolation, and qPCR were as described previously.[40]

sgRNA sequences:
Notch1_exon3: AGTGCCGCTGCCCACCAGGG.
Notch1_exon5: TACATACCCGTCCACTCCGG.
ROSA26: CTCCAGTCTTTCTAGAAGAT.

METHOD DETAILS

Acquisition and processing of human glioma samples for single cell RNAseq

Fresh tumors were collected at the time of surgery and presence of glioma was confirmed by frozen section. Tumor specimens were mechanically dissociated with a disposable, sterile scalpel and further enzymatically dissociated into single cell suspensions using the enzymatic brain dissociation kit (papain-based) from Miltenyi Biotec as previously reported.[20,21,41,42] Tumor cells were blocked in 1% bovine serum albumin in phosphate-buffered saline solution (1% BSA / PBS). Cell suspensions were subsequently stained for flow cytometry for 30 min at 4°C using antibodies specific for CD45 [REA747]-VioBlue and CD3 [BW264/56]-PE from Miltenyi Biotec. Cells were washed with cold PBS, and then incubated for 15 min in 1.5 mL of 1% BSA / PBS containing 1 uM calcein AM (Life Technologies) and 0.33 uM TO-PRO-3 iodide (Life Technologies). Sorting was performed with the FACS Aria Fusion Special Order System (Becton Dickinson) using 488 nm (calcein AM, 530/30 filter; CD3-PE, 585/42 filter), 640nm (TO-PRO-3, 670/14 filter), and 405 nm (CD45-VioBlue, 450/50 filter) lasers. Standard, strict forward scatter height versus area criteria were used to discriminate doublets and gate only singleton cells. Viable cells were identified by staining positive with calcein AM but negative for TO-PRO-3. We sorted individual, viable, CD45^{+}CD3- and CD45^{+}CD3^{+} immune, and CD45- non-immune single cells into 96-well plates containing cold TCL buffer (QIAGEN) with 1% beta-mercaptoethanol. Plates were frozen on dry ice immediately after sorting and stored at -80°C prior to whole transcriptome amplification, library preparation and sequencing.

RNA *in situ* hybridization

Paraffin-embedded tissue sections from human tumors from Massachusetts General Hospital were obtained according to Institutional Review Board-approved protocols. Sections were mounted on glass slides and stored at −80°C. Slides were stained using the RNAscope 2.5 HD Duplex Detection Kit (Advanced Cell Diagnostics, Cat. No. 322430). Slides were baked for 1 h at 60°C, deparaffinized and dehydrated with xylene and ethanol. The tissue was pretreated with RNAscope Hydrogen Peroxide (Cat. No. 322335) for 10 min at room temperature and RNAscope Target Retrieval Reagent (Cat. No. 322000) for 15 min at 98°C. RNAscope Protease Plus (Cat. No. 322331) was then applied to the tissue for 30 min at 40°C. Hybridization probes were prepared by diluting the C2 probe (red) into the C1 probe (green). The ratio of C2:C1 was 1:50 for MKI67/SOX4 and 1:60 for GFAP/ALDOC. Advanced Cell Technologies RNAscope Target Probes used included Hs-GFAP-C2 (Cat No. 311801-C2), Hs-ALDOC (Cat No. 407031), Hs-SOX4 (Cat No. 469911), Hs-MKI67-C2 (Cat No. 591771-C2). Probes were added to the tissue and hybridized for 2 h at 40°C. A series of 10 amplification steps were performed using instructions and reagents provided in the RNAscope 2.5 HD Duplex Detection Kit. Tissue was counterstained with Gill's hematoxylin for 25 s at room temperature followed by mounting with VectaMount mounting media (Vector Laboratories). For RNA *in situ* hybridization quantification, at least 1,000 cells were counted across 10 high power fields in representative areas of the tumors.

Processing of matched pre- and post-treatment samples for single-cell RNAseq

For each sample, a piece of frozen tumor tissue (approximately 5mm x 5mm x 5mm) was placed into a well of a 6-well plate (Corning, Cat. No. CLS3516-50EA) containing 1 ml of CST buffer and processed on ice. Tumor tissue was chopped for 10 minutes using Noyes Spring Scissors (Fine Science Tools, Cat. No. 15514-12). The sample was then filtered through a 40 um cell strainer (Fisher Scientific, Cat. No. 22363547) and the well and filter were washed with an additional 1 ml of CST buffer. The total volume was then brought up to 5 ml with 3 ml of ST buffer and the sample was centrifuged in a 15 ml conical tube at 4°C for 5 minutes at 500 g. The supernatant was removed and the pellet was resuspended in 100 ul ST buffer. The sample was then filtered through a 35 um cell strainer (Falcon, Cat.

No. 352235). Nuclei suspension was counted using disposable C-Chip Hemocytometers (INCYTO, Cat. No. DHCN012). Single nuclei were processed through the 10X Chromium 3' Single Cell Platform using the Chromium Single Cell 3' Library, Gel Bead and Chip Kits, following the manufacturers protocol. Briefly, 8,000 single nuclei were loaded into each channel of the chip to be partitioned into Gel Beads in Emulsion (GEMs) in the Chromium instrument, followed by nuclei lysis and barcoded reverse transcription of RNA in the droplets. This was followed by amplification, fragmentation, and addition of adaptor and sample index. Libraries from two 10x channels were pooled together and sequenced on one lane of an Illumina Next-Seq 500 sequencer with paired end reads, Read 1: 28 nt, Read 2: 55 nt, Index 1: 8 nt, Index 2: 0 nt. Buffers for nuclei preparation were prepared as follows. ST buffer: Salt-Tris solution containing 146 mM NaCl (Thermo Fisher Scientific, Cat. No. AM9759), 10 mM Tris-HCl pH 7.5 (Thermo Fisher Scientific, Cat. No. 15567027), 1 mM CaCl2 (SigmaAldrich, Cat. No, 21115) and 21 mM MgCl2 (Sigma Aldrich, Cat. No. M1028) in ultrapure water. CST buffer: 10 ml of ST buffer, 320 μl of 0.25 M CHAPS (Thermo scientific, Cat. No. 28300) and 10 μl of 10% BSA (Sigma Aldrich, Cat. No. A3059).

NCT03343197 RNAseq data acquisition and pre-processing

The bulk RNAseq profiles generated by Mellinghoff et al.[30] were obtained with the dbGAP accession no. phs003148.v1.p1. Read fragments of bulk RNAseq were mapped against the GRCh38 genome using STAR (version 2.7.10a) with the following parameters (default otherwise): –outFilterMultimapNmax20 –alighSJoverhangMin8 –alignMatesGapMax 1000000 –alignIntronMax 1000000 –twopassMode Basic. The number of read counts were generated for each annotated gene using STAR –quantmode Genecounts output.

Single-cell RNAseq and single-cell muti-omics data generation of mouse glioma model

Idh^{R132H} mouse glioma cells with *Notch1*-KO and *Notch1*-WT were cultured in the presence of 1 μM AG-881or vehicle (DMSO control) for > 2 weeks. The treated cells were washed with cold PBS and then stained with 1 uM calcein AM (Life Technologies) and 0.33 uM TO-PRO-3 iodide (Life Technologies) for 30 min at 4°C. Sorting was performed with the FACS Aria Fusion Special Order System (Becton Dickinson) using 488 nm (calcein AM, 530/30 filter) and 640nm (TO-PRO-3, 670/14 filter). Side scatter (SSC) width versus forward scatter (FSC) area, and Trigger Pulse Width versus FSC criteria were used to discriminate doublets. Calcein AM positive and TO-PRO-3 negative live cells were sorted into the collection tubes for scRNA-seq and into 96 wells containing TCL buffer (QIAGEN) for the single-cell multi-omics experiment. The single-cell suspension for *Notch1*-KO and *Notch1*-WT mouse glioma cells treaded by AG-881 or DMSO (8,000 cells per group) were profiled by the 10X Chromium 3' Single Cell Platform and were sequenced as already mentioned. The single-cell plates for the mouse glioma cells treaded by AG-881 or DMSO were profiled by the joint single-cell RRBS and whole transcriptome amplification (Smart-seq2) protocol. The library preparation and sequencing were performed as previously described.[32] Single enzyme digestion (MspI) was used to enrich CpG dense regions in single-cell RRBS.

QUANTIFICATION AND STATISTICAL ANALYSES

Single-cell RNAseq data processing of human glioma samples

Smart-seq2 whole transcriptome amplification, library construction, and sequencing were performed as previously published.[20,21,41,42] We processed sequencing data from raw reads to gene expression matrices as previously described.[20] We used bcl2fastq to generate demultiplexed FASTQ files, and aligned the resulting paired-end scRNA-seq reads to the human transcriptome (hg19) using Bowtie (v0.12.7).[43] Statistical analysis was done using *R* version 4.0.1. We merged the gene expression levels which were calculated by RSEM[44] for MGH170 and MGH229 with the ones calculated for the reference samples from *Tirosh* et al. *2016*[20] (downloaded from https://singlecell.broadinstitute.org/single_cell). Analysis was done mainly using the R package *scandal* which is freely available at https://github.com/dravishays/scandal. Gene expression levels were quantified as $E_{i,j} = log\,2\left(\frac{TPM_{i,j}}{10} + 1\right)$ where $TPM_{i,j}$ refers to transcript-per-million for gene *i* in sample *j*. We divided the *TPM* values by 10 as the size of single-cell libraries is estimated to be in the order of 100,000 transcripts and we therefore would like to avoid inflating the expression levels by counting each transcript ~10 times. We filtered out cells with fewer than 3000 detected genes yielding 1153 IDHi-treated cells and 4334 untreated cells (Table S2). Next, we computed the average expression of each gene *i* as $log\,2\left[\left(\frac{1}{n}\sum_{j=1}^{n} TPM_{i,j}\right) + 1\right]$ in each tumor sample separately and excluded genes with average expression below 4. We then merged the gene lists from the 8 tumor samples, leaving a set of 10516 genes for downstream analysis. For the cells and genes that passed these quality control procedures we defined relative expression levels by centering the expression levels for each gene across all cells in the dataset as follows: $Er_{i,j} = E_{i,j} - \frac{1}{N}\sum_{k=1}^{N} E_{i,k}$ where *N* is the number of cells in the dataset.

Clustering and identifying presumed normal and malignant cells

We clustered all cells using graph-based clustering (Louvain's algorithm) of a 2-dimensional UMAP space (R's UMAP package, distance metric set to "pearson") computed from the relative expression levels. We identified two small clusters containing cells highly expressing markers of Oligodendrocytes and Macrophages which were annotated accordingly, whereas the rest of the cells were annotated as presumed malignant (Figure 1C).

Please cite this article in press as: Spitzer et al., Mutant IDH inhibitors induce lineage differentiation in IDH-mutant oligodendroglioma, Cancer Cell (2024), https://doi.org/10.1016/j.ccell.2024.03.008

CNA analysis

CNAs were estimated as described elsewhere.[20,21,28,41,42] Briefly, the algorithm sorts the analyzed genes according to their chromosomal location and applies a moving average with a sliding window of 100 genes within each chromosome to the relative expression values. The scores computed for the cells classified as non-malignant (Oligodendrocytes and Macrophages in this case) define the baseline of normal karyotype and their average CNA values are used to center the values of all cells. Classification of cells as malignant/non-malignant was based on two metrics:

1. CNA signal: reflects the extent of CNAs in each cell, and defined for each cell j as $\frac{1}{n}\sum_{i=1}^{n} CNA_{i,j}^{2}$ where n is the number of genes and.
2. CNA correlation: defined as the Pearson correlation between the CNA profile of each cell and the average CNA profile of all presumed malignant cells from the corresponding tumor sample.

Cells were classified as malignant if CNA signal was above 0.025 and CNA correlation was above 0.25. Cells that failed to pass the two thresholds were marked as "unresolved" and excluded from downstream analysis.

Gene-sets associated with malignant cellular states

For scoring samples (including TCGA samples) we used gene-sets curated from Tirosh et al. 2016[20] denoted here as the IDH-O AC-like, OC-like, NPC-like, G1/S and G2/M programs. For functional annotation of gene lists such as in Figure 2A we also included gene-sets curated from Venteicher et al. 2017[21] and Neftel et al. 2019.[28] See the gene-sets in Table S2.

Gene-sets associated with normal brain cell types

We scored the tumor samples for gene-sets representing normal cell types which were curated from published scRNA-seq datasets.[22–27] Each dataset was converted to CPM units (if not already in TPM units) and log2-transformed. Genes were filtered by *Ea* with a mean expression cutoff of 4. Gene-sets were then defined by differential expression between the clusters that were defined in the respective paper. We selected the top 50 genes by log2 fold-change (FC), with log2FC>=1 and Benjamini-Hochberg adjusted p-value<0.05. See the gene-sets in Table S2.

Assignment of cells to states

Malignant cells were scored for the *IDH-O AC-like*, *OC-like* and *NPC-like* programs using the function *sigScores* from the R package *scalop* available at https://github.com/jlaffy/scalop. We generated 100 shuffled expression matrices by sampling each time 1000 cells and shuffling the expression values for each gene. We then scored each shuffled matrix for the AC-like, OC-like and NPC-like expression programs, thus yielding 100,000 normally distributed scores for each expression program. These were used as null distributions for cell state classification. For each original cell, we computed a p-value for each of the expression programs with a Z-test (R's *pnorm* function) using the statistics of the null distributions that we previously generated. We adjusted all p-values for multiple testing using the Benjamini-Hochberg method. Each cell was classified into a specific state if the adjusted p-value computed for that state was smaller than 0.05. Cells that either did not achieve an adjusted p-value < 0.05 for any of the states or achieved an adjusted p-value < 0.05 for multiple states (~6% of cells) were assigned an "Undifferentiated" state. See Figure S1D for the statistics of state assignment for each sample.

Cell cycle analysis

Malignant cells were scored for the *IDH-O G1/S* and *G2/M* programs and classified as cycling using the same method described above for cell state classification. See Figure S1C for the statistics of cell cycle assignment for each sample.

Gene-set enrichment analysis

For each sample s we computed a bulk expression profile for each gene i as $log_2\left(\frac{1}{n}\sum_{j=1}^{n} TPM_{i,j}+1\right)$ where n is the number of cells in sample s. We then computed the average log_2 expression of each gene across the IDHi-treated and untreated samples and then computed the $\log_2$-ratio of each gene by subtracting the average $\log_2$ expression of the untreated samples from that of the treated samples. We then generated the ranked list used for GSEA[45,46] by sorting the $\log_2$-ratio list. GSEA was computed using the R package *fgsea*.[47] We included in this analysis 10264 gene-sets (10185 GO gene-sets, 50 mSigDB hallmark gene-sets, 11 gene-sets reflecting Glioma cellular hierarchy and 18 gene-sets reflecting normal astrocytic, oligodendrocytic and OPC development) which were downloaded from mSigDB or curated as described above.

Ranked list enrichment analysis (pertaining to Figure 2B)

Ranked list genes (see Gene-set enrichment analysis) were annotated according to inclusion in AC-like, OC-like and NPC-like gene-sets curated as described above. We computed the fraction of genes associated with a particular state in windows of 30 genes at fixed intervals of 0.25 along the spectrum of log2-ratio values (ranging from -2.5 to 2.5). See Table S2 that contains the computed fractions.

Please cite this article in press as: Spitzer et al., Mutant IDH inhibitors induce lineage differentiation in IDH-mutant oligodendroglioma, Cancer Cell (2024), https://doi.org/10.1016/j.ccell.2024.03.008

Combined DEG analysis of unmatched and matched cohorts

As before-mentioned, the unmatched and matched cohorts were analyzed separately, yielding two lists of DEGs (for the unmatched cohort by comparing the bulk expression profiles of the IDHi-treated samples with those of the untreated samples and for the matched cohort by comparing the expression profiles of the on- and pre-treatment samples). From each of these lists we included in the analysis the 5% most upregulated and 5% most downregulated genes (e.g. 10% of genes) and generated the combined DEG list by intersecting the two lists.

Permutation test for OPC-OC differentiation (pertaining to Figure S4D)

Malignant cells were scored for normal OC and OPC programs curated from normal brain datasets as discussed above. We computed the difference between the two scores for each cell and then averaged the score difference per sample. We then computed a sampling distribution of the mean *OC-OPC* score difference by generating 1000 random gene expression matrices as described above. We scored each of these shuffled matrices for the normal OC and OPC expression programs and then counted how many times the mean score difference of each sample was greater than that of the shuffled matrices. For each sample a p-value was computed as $1 - \frac{n}{N}$ whereas n is the number of times the mean score difference of the particular sample was higher than that of the shuffled matrices and N is the number of repeats (1,000). The p-values were corrected for multiple testing for each program using the Bonferroni method.

Assessment of the relative change in proportions of cell states in IDHi-treated vs. untreated samples

For each state $s \in \{AC-like, OC-like, Undifferentiated/NPC-like, Cycling\}$ and for each pair of IDHi-treated and untreated samples, $t \in \{MGH170, MGH229\}$ and $u \in \{MGH36, MGH53, MGH54, MGH60, MGH93, MGH97\}$, we defined Ft,s and Fu,s as the fraction of cells assigned to state s in samples t and u respectively and computed $R_{t,u,s} = log\,2\left(\frac{F_{t,s}}{F_{u,s}}\right)$ which represents the relative difference in the proportion of cells assigned to state s in the IDHi-treated sample t compared with the untreated sample u in log2FC units. Statistical significance of the difference was tested with a hypergeometric test (fisher.test function implemented is R's stats package) for each (s, t, u) combination and corrected for multiple testing using the Benjamini-Hochberg method (p.adjust function implemented in R's stats package).

Single-cell RNAseq data processing of matched pre- and post-treatment samples

Illumina sequencing base calls were converted into FASTQ files using *cellranger* v4.0.0 pipeline (*mkfastq* command). Gene expression matrices were generated using *cellranger* (*count* command) by aligning the FASTQ files to a pre-mRNA reference transcriptome (GRCh38 GENCODE v32/Ensemble 98) which was built according to instructions provided by 10x Genomics. Each of the matched pairs was analyzed independently (pre- and post-treatment samples from the same pair were analyzed together) and the same analysis steps were applied to both of them. Expression data of each matched pair was normalized, clustered and annotated (for cell types) using the *Seurat* package.[48] Malignant cells were detected using CNA analysis and classified into cell states as described above.

NCT03343197 RNAseq data analysis

Raw gene counts were transformed into counts-per-million (CPM) scale and log2-transformed as log2(CPM+1). Mean expression values (E) were computed for each gene by averaging across the CPM values and genes with $\log2(E+1)$ less than 4 filtered out, leaving 8,561 genes for analysis. Samples that did not have the 1p/19q co-deletion based on the clinical annotation file were filtered out, leaving us with 23 samples. Finally, we defined relative expression levels by gene-wise centering of the *log2(CPM+1)* expression values.

TCGA data preprocessing

Gene expression data (raw counts), clinical annotation file and mutation annotation file for the TCGA-LGG project were downloaded using the R package *TCGAbiolinks*.[49] We filtered out genes with low variability, leaving 10,000 genes for analysis. Raw gene counts were transformed into counts-per-million (CPM) scale and log2-transformed as log2(CPM+1). We filtered out samples that do not have the 1p/19q co-deletion based on the clinical annotation file, leaving us with 150 samples. Since tumor grade may impact certain aspects of the analysis we filtered out 16/150 samples from the dataset for which grade annotation was not available in the clinical annotation file. Finally, we defined relative expression levels for each dataset separately by gene-wise centering of the *log2(CPM+1)* expression values.

Bulk scoring of TCGA samples

We scored the TCGA samples using the centered log2(CPM+1) values for the AC-like, OC-like, NPC-like and cell-cycle programs (same gene-sets that were used for scoring the single-cell data) by computing the mean expression per sample for each program.

TCGA AC differentiation analysis

We computed for each sample an AC-differentiation score, defined as $AC_{diff} = AC - \frac{OC+NPC+CC}{3}$ where AC, OC, NPC and CC represent the sample's scores for the AC-like, OC-like, NPC-like and cell-cycle programs. This enabled deriving an expected AC differentiation score for each tumor grade $g \in \{Grade\ 2, Grade\ 3\}$ which is the average AC differentiation score across all samples that

Please cite this article in press as: Spitzer et al., Mutant IDH inhibitors induce lineage differentiation in IDH-mutant oligodendroglioma, Cancer Cell (2024), https://doi.org/10.1016/j.ccell.2024.03.008

belong to grade *g*. Since tumor grade may impact the degree of AC-like differentiation, we compared the differentiation score distributions of grade 2 and grade 3 tumors and indeed found that grade 2 tumors were, on average, more differentiated than grade 3 tumors (p=0.0008, Wilcoxon rank sum test). We defined bulk expression profiles for each of the samples analyzed by scRNA-seq by averaging across the cells in each tumor and computed AC differentiation scores for these samples as well using the bulk expression profiles. These scores span the expected spectrum of AC differentiation within the TCGA cohort (Figure S5A). This property enabled using the expected AC differentiation computed from the TCGA to compute relative AC differentiation scores and account for differences in tumor grade. These scores were defined for each sample *i* as $ACdiff_i$ - *E(ACdiff)* where *E(ACdiff)* is the expected AC differentiation score corresponding to sample *i*'s tumor grade.

Mutations associated with changes in AC differentiation

TCGA data was separated into two datasets according to tumor grade. Each dataset was row-centered, scored for the AC-like, OC-like and NPC-like programs and the AC differentiation score was computed. We included in this analysis only mutations with at least 5 occurrences in a particular dataset (according to the mutation annotation file). For each mutation we computed the difference between the mean AC differentiation scores of the samples with the mutation and those without the mutation (relative AC differentiation score) and the statistical significance of the difference between the two groups using Wilcoxon rank sum test (corrected for multiple testing using the Benjamini-Hochberg method).

Single cell DNA methylation analysis

Analysis of single cell DNA methylation was performed based on the methods detailed in Chaligne et al.[33] After demultiplexing, reads were mapped to the mm10 genome and cells with at least 25,000 CpG sites, 1 million reads and mapping efficiency greater than 30% were retained for downstream analysis. Differentially methylated promoters were based on the 1kb region around promoters from GENCODE M33 (GRCm39 release) and the FANTOM database of enhancers. Significantly methylated regions were determined based on an adjusted p-value less than 0.05 and methylation difference of 10% between conditions (IDHi and DMSO).

Multi-omics data analysis

Gene-set enrichment analysis was performed separately for the top 100 de-methylated and top 100 upregulated genes using ~3000 gene-sets that include GO terms and gene-sets from normal brain development and glioma hierarchy. For each gene-set we computed the observed overlap (i.e. overlap between gene-set and top demethylated/upregulated genes) and the expected overlap (i.e. overlap between gene-set and list of genes that passed QC). P-values were computed for each gene-set using a Fisher test.